hydrology

MDPI

Article

Impact of Hydrometeorological and Climatic Pressures on Greek Rivers: Implementation into the Water Framework Directive 2000/60

Angeliki Mentzafou [1,2,*], Elias Dimitriou [1], Anastasios Papadopoulos [1] and Petros Katsafados [2]

[1] Hellenic Centre for Marine Research—H.C.M.R., Institute of Marine Biological Resources and Inland Waters, 46.7 km Athens—Sounio Ave., 19013 Anavyssos, Attica, Greece; elias@hcmr.gr (E.D.); tpapa@hcmr.gr (A.P.)
[2] Department of Geography, Harokopio University of Athens, 17671 Kallithea, Attica, Greece; pkatsaf@hua.gr
* Correspondence: angment@hcmr.gr; Tel.: +30-2291076349

Abstract

Rivers are vulnerable to hydrometeorological and climatic pressures, while effective water resources management during low-flow season can be challenging. This paper studies the impacts of extreme hydrometeorological events and climate change on Greek rivers, and presents a framework for the incorporation of these pressures into the Program of Measures (PoMs) of the River Basin Management Plans (RBMPs) for the implementation of the Water Framework Directive 2000/60 (WFD). The final aim is the adaptation to drought and water scarcity. The proposed methodological approach incorporates a process-based model, climate change projections, drought indices and low-flow boundaries, so as to assess the impact of hydrometeorological and climatic pressures on the quantitative quality status of rivers. Then, the quantitative response of rivers under different predicted climate scenarios was examined. Based on the results, a water management plan was adopted and tested regarding its effectiveness, so as to promote evidence-based water strategies. Additionally, comprehensive measures and an operational scheme and adaptations actions for the mitigation of the hydrometeorological and climate related pressures in rivers of Greece were proposed. This operational framework is based on quantitative thresholds that trigger actions and measures for adaptation and can be used by decision-makers and stakeholders as guidelines for mitigation actions. The framework proposed was applied to the Spercheios river basin, which was selected as a demonstration site.

Keywords: hydrometeorological extremes; drought; water scarcity; low-flow boundaries; climate change projections; program of measures; water resilience; climate adaptation; hydrological model; Spercheios river

Check for updates

Academic Editors: Dejana Jakovljević, Dragana Milijašević Joksimović, Ana Milanović Pešić and Alina Bărbulescu

Received: 16 July 2026
Revised: 19 August 2026
Accepted: 26 August 2026
Published: 28 August 2026

Copyright: © 2026 by the authors. Licensee MDPI, Basel, Switzerland. This article is an open access article distributed under the terms and conditions of the Creative Commons Attribution (CC BY) license.

1. Introduction

Rivers constitute the natural course of freshwater that flows on the earth's surface or partially subterranean toward a reference point (sea, inland reservoirs, lakes, other rivers, or caves) [1,2]; they are highly biodiverse, contribute to the global biogeochemical cycles, and provide valued and multiple socioeconomic services [3]. Riverine ecosystems are complex and characterized by both spatial and temporal variability [4]. They do not simply function as means of transporting water, chemicals and sediment, but are also ecosystems in which all the diverse and complex processes between their abiotic and biotic components take place [2]. The key factor affecting the conditions and the habitat of the riparian zone and floodplains of rivers is their natural hydrological regime [5], which is the flow regime of the watercourse

controlled by the characteristics and the climatic conditions of the river basin alone, without any anthropogenic interventions [6]. Consequently, deviations from the natural hydrological regime of a river, due to pressures related to human activities, directly affect the river health and the structure of biological communities or the natural environment [7,8].

Hydrometeorological pressures in rivers refer to extreme weather events (i.e., short-term, typically ranging from minutes to a few days), such as floods and droughts. Climatic pressures (i.e., long-term, generally ranging between annual and decadal periods) are associated with changes and trends in weather statistics [9,10]. Climate change, and hydrometeorological or climatic pressures, increase and aggravate stress on surface waterbodies [11–13] and impact freshwater ecosystem functionality [14]. Climate change, in combination with anthropogenic activities, especially water abstractions and land use changes, is predicted to impact river flow magnitude and lead to a decrease in streamflow in Southern Europe [15]. In the Mediterranean, especially in the southern and eastern parts, a decrease in surface runoff and low flows, probably by 12–15%, and a change in seasonality, with an increase in winter flows due to increased precipitation (and reduced snowfall) and a decrease in summer flows, are expected [16,17]. Overall, climate change is projected to impact rivers' flow regime more severely than anthropogenic activities such as water abstractions, land use change and hydro-technical installations [14,18]. Likewise, hydrometeorological extremes, and droughts in particular, are expected to be intensified due to global warming [19]. In the Mediterranean region, meteorological droughts, which are related to reduced precipitation, when prolonged may lead to extreme soil moisture deficit, and eventually to water scarcity and streamflow decrease (hydrological drought) [17]. Moreover, in all emission scenarios examined, a more profound increase in hydrological drought duration, frequency and intensity has been predicted [19,20], mainly due to the additional anthropogenic pressures applied [21]. Eventually, hydrometeorological extremes and climate change-related flow regime alteration, and especially low flow disruption, are expected to impact freshwater biogeochemical processes. Consequently, biodiversity and species compositions, as well as water quality status and river health and integrity, are expected to be impacted [22–24].

Effective water resource management during the low-flow season [25,26], and especially under such changing environmental conditions, can be challenging [27,28]. The Water Framework Directive 2000/60 (WFD) [29], along with other European Union (EU) policies such as the Nitrate Directive (ND) [30], the Floods Directive 2007/60/EC (FD) [31], and the Drinking Water Directive 2020/2184 (DWD) [32], provide the framework for the protection of water resources and ecosystem-based water management [33]. Long-term water resource strategies and management plans must also be adjusted to address hydrometeorological extremes and climate change pressures, and incorporate climate change impact assessment, while accommodating water needs and ensuring access to sufficient and high-quality water [34,35]. Likewise, the recent European Water Resilience Strategy (WRS) focuses on the efficient implementation of the WFD, and on the promotion of a water-smart economy, so as to address water scarcity and quality degradation even under uncertain future climate conditions [36]. To ensure the potency of management plans and the effectiveness of policies and measures, climate change must be considered during the determination of priority actions and the development of the program of measures (PoMs) within the framework of River Basin Management Plans (RBMPs) mandated by the WFD/Article 11 [13].

As outlined in the EU Strategy on Adaptation to Climate Change, the improvement of knowledge and the understanding of possible climate change impacts on water resources are essential for comprehensive assessments [37]. Long-term and continuous water monitoring and reporting, as dictated by the WFD, are vital for the evaluation of water management plans and climate change adaptation [33,38], as well as for the restoration of the water cycle [36]. Additionally, hydrological models constitute a valuable tool in

understanding and forecasting the impact of climate change and hydrometeorological pressures on surface waterbodies and water resources. Likewise, hydrological models support decision-makers and stakeholders in the development of sustainable management plans, and the assessment and the identification of adaptation options [33,36,37,39–41]. In Greece, the National Climate Change Adaptation Strategy (NCCAS) and the Regional Adaptation Action Plans (RAAPs) dictate the necessity for the adoption of policies and innovative technologies and practices that promote rational water resource management [38,42,43]. NCCAS and RAAPs also promote the integration of climate change in water resource management and plans, and into the PoMs, and the quantitative impact assessment of possible scenarios using models [44].

This study aims to improve the understanding of climatic pressures and hydrometeorological extremes in the rivers of Greece, so as to contribute to the development of a framework for the integration of climate change impacts into the PoMs of the RBMPs for the implementation of the WFD (Figure 1). The methodological approach presented in this study incorporates process-based models, climate change projections, drought indices and the national low-flow thresholds established in a previous study [45], in order to assess the impact of hydrometeorological and climatic pressures on the quantitative and qualitative status of rivers. More specifically, the introduced framework employs physically based hydrological models and long-term meteorological forecasts for forcing the hydrological model. Meteorological and hydrological drought indices are used to identify the impact of climate change-related hydrometeorological pressures in rivers. Additionally, the low-flow thresholds distinguishing moderate- from good-quality status, defined in a previous study to support the implementation of WFD in Greece [45], are also employed. Then, the quantitative response of rivers under different predicted climate scenarios can be examined. The analysis can be performed on the existing monitoring network established to fulfill the obligations arising from the WFD regarding reporting the water status of surface waterbodies [46]. Additionally, based on the results, a water management plan can be adopted and tested for its effectiveness, so as to promote evidence-based water strategies. The main scope of the present study was to provide guidelines to incorporate climate change impacts and hydrometeorological extremes in rivers into the PoMs of RBMPs for the implementation of the WFD in Greece based on quantitative assessments (Figure 1).

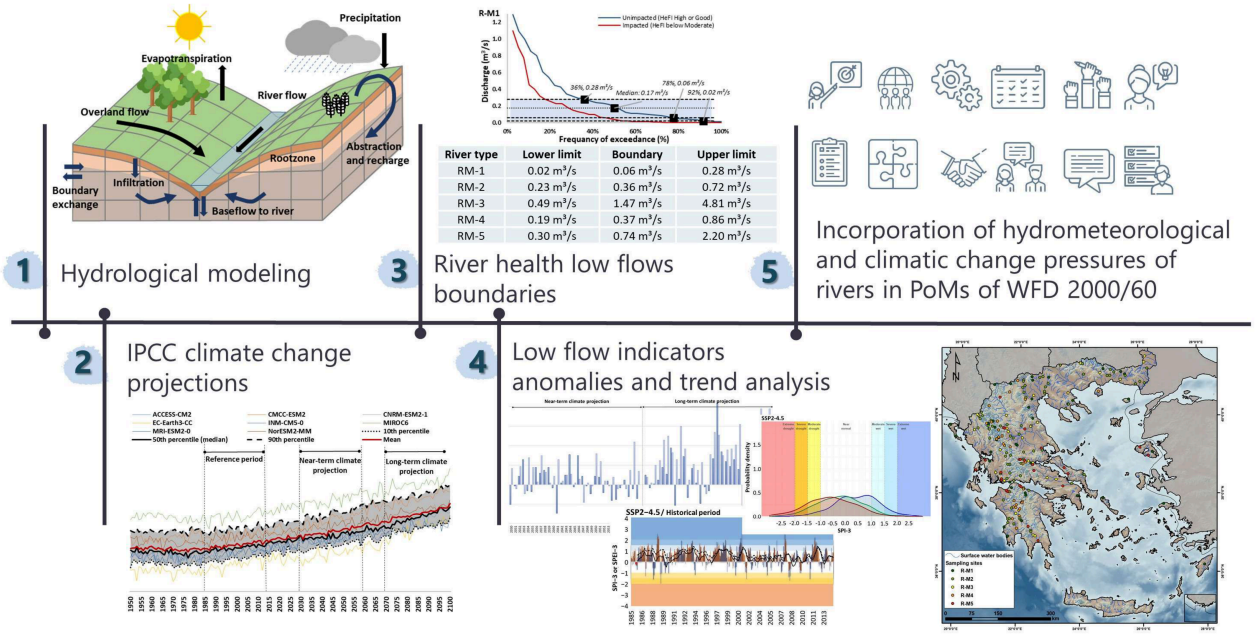

River type	Lower limit	Boundary	Upper limit
RM-1	0.02 m³/s	0.06 m³/s	0.28 m³/s
RM-2	0.23 m³/s	0.36 m³/s	0.72 m³/s
RM-3	0.49 m³/s	1.47 m³/s	4.81 m³/s
RM-4	0.19 m³/s	0.37 m³/s	0.86 m³/s
RM-5	0.30 m³/s	0.74 m³/s	2.20 m³/s

Figure 1. Schematic overview of the study design.

The proposed framework was applied to the Spercheios river basin, which was selected as a case-study. The specific area is characterized by a variety of anthropogenic activities and impacts (agricultural activities, water diversion, land use changes, water abstractions, etc.) that affect the hydrological regime of the river. Additionally, the geomorphology of the Spercheios river basin is characterized by the transition from mountainous terrain upstream to a flood plain downstream. Therefore, the specific area provides the necessary variability of hydrological regime along the river course, since the hydrographic network comprises temporary streams, torrential watercourses, and eventually perennial rivers [47]. Finally, the Spercheios river basin is susceptible to climate change impacts (high risk of climate change) [48], and is vulnerable to hydrometeorological-related hazards [49].

2. Materials and Methods

2.1. Case Study

2.1.1. Study Area

Spercheios river basin is located at the administrative region of Central Greece, in the regional unit of Fthiotida (Figure 2). The river basin under study has an almost eastern–western direction, and covers an area of about 1660 km^2, while Spercheios river has an extensive hydrographic network and flows towards Maliakos Gulf at the western part of the Aegean Sea to the east. The mean area-weighted annual spatial distributed precipitation of the catchment area for the period 1981–2020 has been estimated to be about 815 mm. Following the Köppen–Geiger climatic characterization, the study area is under a Mediterranean Climate, in Csa class, indicating a dry warm period and a wet period distributed from late autumn to early spring. Spercheios river's main course has a total length of approximately 90 km, while its annual discharge fluctuates between 2 and 100 m^3/s, with an average value of about 22 m^3/s [50].

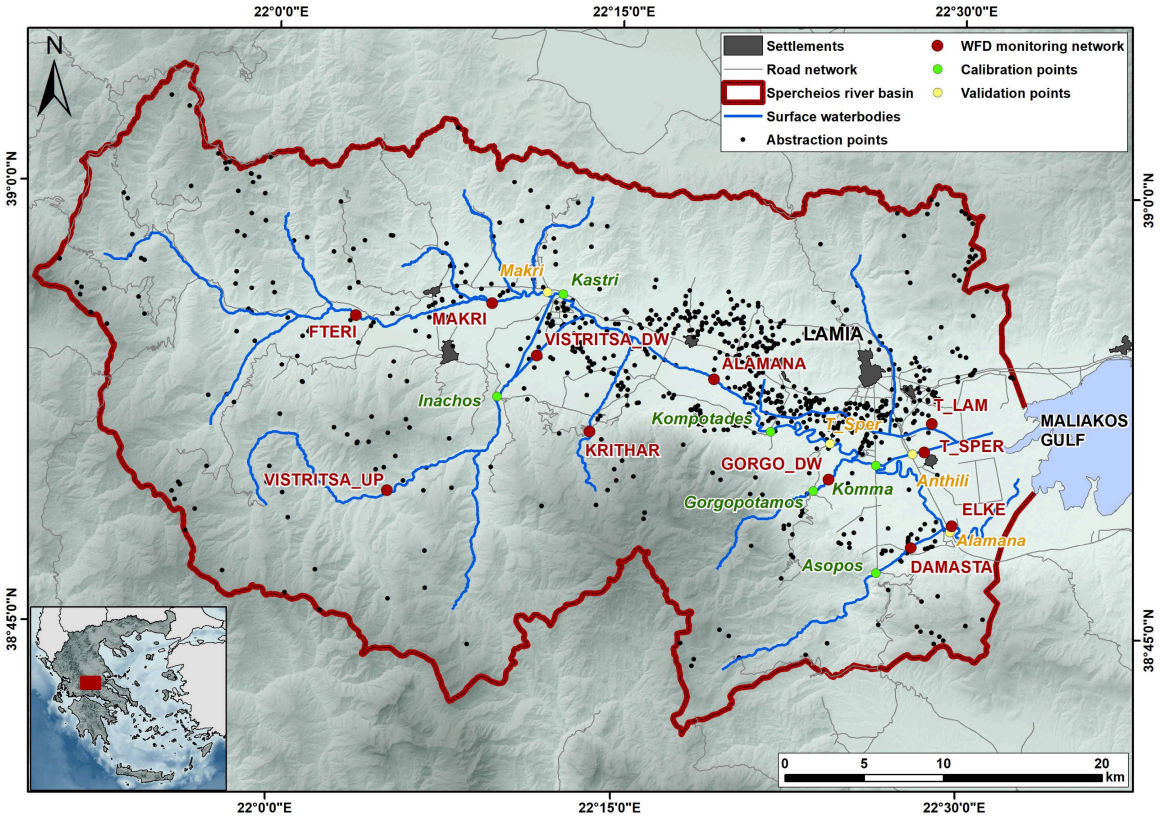

Figure 2. Spercheios river basin with the main water abstraction points, the calibration/validation points of the hydrological model and WFD river monitoring network.

The Spercheios river watercourse has been subjected to multiple alterations throughout its history, mainly due to tectonic and sediment erosion–depositional mechanisms [51–53]. The most important morphogenetic processes affecting the landscape of Spercheios valley are endogenic. The neotectonic graben of the basin is bounded firstly by west/northwestern–east/southeastern- and secondly by east/northeastern–west/southwestern- and/or northeastern–southwestern-directed fault systems [54,55], while a geothermal field is located at the southeastern part of the basin [56,57]. Additional exogenic processes contribute to the high erosion rate and sedimentation [47,53,58]. The dominant geological formation of the Spercheios river basin is the semi-permeable to impervious flysch that structures the mountainous regions surrounding the valley. The alluvial plain is formed by quaternary deposits (clays, sands, gravels, talus, and coastal conglomerates) of variable permeability. Finally, the northern part of the basin and the northeastern and southern parts of the basin are locally structured by impervious plutonic and volcanic rocks and highly permeable karstic formations, respectively [59].

The watershed of Spercheios river has been subjected to numerous anthropogenic interventions. These, along with the natural endogenic and exogenic processes mentioned above, form a dynamic river course and deltaic system that have undergone multiple hydromorphological changes during its evolution. Engineering interventions, such as land reclamation projects and irrigation networks, drainage ditches, flood control channels, canalizations, erosion control projects, and streambank stabilization practices, have altered the natural river course and have destabilized the coastline [47,51,53,58,60].

2.1.2. Hydrological Simulation

The modeling tool used in the present study was the MIKE SHE 2025 developed by the Danish Hydraulic Institute Water and Environment—DHI Water and Environment [61]. MIKE SHE is a physically based distributed model that is able to simulate all hydrological domains within the land phase of the hydrological cycle in a river basin [62] and has been frequently and successfully used to simulate ecohydrological processes [63]. This integrated modeling tool can simulate overland flow, unsaturated flow, vegetation-based evapotranspiration, groundwater flow and fully dynamic channel flow. Additionally, it can describe their hydraulic relationship, while it can also simulate integrated water quality throughout the hydrologic cycle [61]. MIKE SHE 2025 is fully integrated with the MIKE 1D numerical engine for hydraulic network modeling in MIKE+ Rivers, which is a one-dimensional model that can simulate water flow and level, water quality and sediment transport in rivers, flood plains, irrigation canals, reservoirs and other inland waterbodies. The MIKE 1D hydrodynamic module is based on the complete dynamic wave formulation of the Saint Venant equations [64].

For the needs of the present study, it was essential to further enrich the hydrographic network and extend the calibration/validation period. Eleven branches were eventually included in the model and the time-series for the model setup was prolonged to cover the period 1980–2021. After these improvements, the model was calibrated and validated again. The MIKE SHE 2025 version and MIKE+ Rivers module are more stable than the older one, while all of the errors and bugs reported for the previous releases have been addressed. A cell size of 400 m and a daily time step were used. The final model domain consisted of 10,815 grid points.

The hydrological simulation of Spercheios catchment area was achieved using the following modules: Overland Flow (subcatchment-based surface runoff method); Unsaturated Zone (2-Layer Water Balance Method), Evapotranspiration (Two-Layer UZ/ET model), and Saturated Zone (Linear Reservoir method).

Based on the data availability, the Spercheios model was set up and calibrated for the period October 1980–September 2013 and validated for the period October 2013–September 2021. The Spercheios river basin has already been studied during a past research effort. In that case, the older version of MIKE SHE 2014 and the one-dimensional model for flow simulation MIKE 11 was employed. Additionally, the calibration/validation process focused only on the main river branch and was limited to two and three hydrological years, respectively [65]. Likewise, Spercheios river hydrological model applications have been developed during various past research efforts, but did not focus on the hydrological regime of the river and were not considered appropriate for the purpose of the present study. Past efforts of hydrological modelling of the area focused mainly on the calibration of the monthly water balance components [66], simulated the upper, unimpacted part of the river basin [67], or focused on flood event modelling [68–70].

Details concerning the hydrological model set-up are provided in Appendix A.

2.1.3. Hydrological Model Calibration/Validation

Numerous discharge and water level stations from various agencies and for different time periods have been monitoring the hydrological regime of the Spercheios river network, although usually not in a systematic way (Figure 2, Table 1). In the present study, the calibration and validation periods were set based on the most common split-sample approach in hydrological modelling [71,72], as also dictated by data availability. Therefore, the model was first calibrated for the period 1980–2013 and validated for the period 2014–2021. The validation was performed using a "point-to-point" comparison at the exact matching dates, when in situ observations were available. The calibration of the model was achieved manually, using a trial-and-error procedure between the predicted values and observed measurements, which is the most widely used and recommended method, especially for more complicated models [62]. Although this approach is very time-consuming, tedious, subjective, and requires expertise, it allows the user to better understand the processes of the hydrological system and to identify the strengths and weaknesses of the model [73].

Table 1. Monitoring stations in Spercheios river basin used in calibration and validation of the hydrological model.

Calibration	Owner	Parameter	Start	End	Monitoring Frequency	Latitude (°)	Longitude (°)
Kastri	MEE	Water level	1 October 1980	31 December 2011	Daily	22.211	38.944
Kompotades	MEE	Water level	1 October 1980	30 June 2011	Daily	22.364	38.868
Gorgopotamos	MEE	Water level	1 October 1980	30 June 2011	Daily	22.395	38.834
Komma	MEE	Water level	1 October 1980	30 September 2012	Daily	22.441	38.850
Asopos	RCG	Discharge	11 September 1981	6 September 2010	Monthly	22.421	38.802
Inachos	RCG	Discharge	9 July 997	9 September 2013	Monthly	22.164	38.885
Validation	**Owner**	**Parameter**	**Start**	**End**	**Monitoring Frequency**	**Latitude (°)**	**Longitude (°)**
Alamana	IMBRIW	Water level	3 October 2014	30 June 2020	Daily	22.495	38.813
Anthili	IMBRIW	Water level	6 October 2014	3 September 2021	Daily	22.467	38.856
Makri	ELGO	Discharge	3 July 2012	20 September 2021	Monthly	22.200	38.945
T_Sper	ELGO	Water level	23 October 2013	20 September 2021	Monthly	22.407	38.862

MEE: Ministry of Environment and Energy of Greece. RCG: Region of Central Greece. IMBRIW: Institute of Marine Biological Resources and Inland Waters, Hellenic Centre for Marine Research. ELGO: ELGO Dimitra.

In Table 2, the most important parameters used during the calibration procedure are presented.

The performance of the hydrological model of the Spercheios river basin was evaluated based on the following error metrics: goodness of fit, index of agreement and efficiency criteria: Mean Absolute Error—*MAE*, Mean Square Error—*MSE*, Root

Mean Square Error—*RMSE*, Pearson's correlation coefficient—*R* [74], coefficient of determination—*R*2 [75], Nash–Sutcliffe coefficient—*NSE* [76], Percent bias—*PBIAS*, RMSE to Standard Deviation Ratio—*RSR*, Kling–Gupta efficiency—*KGE* [77,78], Refined Index of agreement—*dr* [79,80].

Table 2. The most important parameters affecting river hydrological regime used in calibration procedure, and their final optimal value.

Parameter	Optimal Value
Land use	
Leaf area index [-] Root depth [mm] Crop coefficient Kc [-]	Spatially and temporally distributed across the model domain
1D	
Manning n [s/m$^{1/3}$] Leakage coefficient [m/s]	0.01–0.10 10^{-14}–10^{-6}
Overland flow	
Slope [-] Slope length [m] Manning Number [m$^{1/3}$/s] Initial Depth [m] Detention storage [mm]	0.0001–0.0005 500–2500 3–8 0.0–0.1 0.1–2.0
Unsaturated zone	
Water content at saturation [-] Water content at field capacity [-] Water content at wilting point [-] Saturated hydraulic conductivity [m/s]	0.36–0.41 0.20–0.25 0.15 5×10^{-8}–1×10^{-5}
Saturated zone	
Interflow reservoirs	
Specific Yield [-]	0.6–0.8
Initial depth [m]	1
Bottom depth [m]	1
Interflow time constant [d]	30–50
Percolation time constant [d]	100–300
Threshold depth [m]	0.95–1.00
Baseflow reservoirs	
Specific Yield [-]	0.005–0.5
Time constant for base flow [d]	1–600
Dead storage fraction [-]	0.05–0.6
UZ feedback fraction [-]	0
Initial depth [m]	0–10
Threshold depth for base flow [m]	0–10
Threshold depth for pumping [m]	0–10
Depth of the bottom of the reservoir [m]	10–20

Details concerning the error metrics and efficiency criteria used in the present study are provided in Appendix B.

Details concerning the hydrological model performance are provided in Appendix C.

The Spercheios river basin is a complex system with multiple natural and anthropogenic pressures affecting the watercourses and the hydrological regime of the surface water. The study area is subjected to neotectonic processes related to the active fault system in mainly the east/northeastern–west/southwestern direction [54,55], the same direction as the Spercheios river. Additionally, complicated erosional/depositional/sedimentological processes [53,58] have subjected the hydrographic network to multiple alterations [51–53].

High irrigation demands during summer lead to water scarcity during these months, while high flood risk during winter related to heavy rainfall events and/or snowmelt jeopardize human lives and infrastructure, and have adverse effects on the ecosystems [81]. Anthropogenic interventions, such as land reclamation projects and irrigation networks, drainage ditches, flood control channels, canalizations, erosion control projects, and streambank stabilization, have altered the natural river course over the years and have destabilized the coastline [47,53,58,60,82].

Due to the high sedimentation rate, flood events, and engineering interventions, the riverbed and the cross-sections of Spercheios river have changed locally several times during recent decades (Figure A6). The impact of these processes on hydrological modeling and prediction accuracy has been acknowledged [83–85]. The MIKE+ River model can be used to indirectly study these dynamic morphological changes by enabling the sediment transport modules [64]. Nevertheless, the lack of sufficient and high-quality data, especially long-term topographic riverbed measurements or high-spatial- and temporal-resolution satellite imagery, as well as sediment load measurements, precludes the development of such a model for Spercheios river basin. Therefore, the cross-sections' temporal geometric alterations were not included in the model and the setup and the calibration were accomplished based on the available cross-sections' geometric information. This can be considered a limitation of the current simulation procedure.

2.2. Climatological Data and Climate Change Scenarios Applied

The Intergovernmental Panel on Climate Change (IPCC) has published six Assessment Reports (ARs) regarding climate science and climate change advances, impacts, and possible adaptation and mitigation measures. The most recent 6th Assessment Report (AR6) presents the climate response to five illustrative scenarios that cover a range of possible future developments of anthropogenic drivers of climate change found in the literature (Socioeconomic Pathways—SSPs) [86]. In the present study, the following two experiments were investigated [87,88]:

- SSP2-4.5 scenario ("Middle of the Road"): intermediate greenhouse gas (GHG) emissions and CO_2 emissions around current levels until 2050, then falling but not reaching net zero by 2100.
- SSP5-8.5 scenario (Fossil-fueled Development—"Taking the Highway"): very high GHG emissions and CO_2 emissions that roughly double from current levels by 2050.

The SSP2-4.5 scenario represents a realistic narrative with medium challenges to mitigation and adaptation, and anthropogenic radiative forcing about 4.5 W/m^2 by 2100 (moderate-forcing sustainable pathway) [87,89]. The SSP5-8.5 scenario describes a pessimistic outlook with high challenges to mitigation and low challenges to adaptation, and with anthropogenic radiative forcing about 8.5 W/m^2 by 2100 (high-end forcing pathway) [87,90].

Projected climate data of the General Circulation Models (GCMs) were developed in the framework of the sixth phase of the Coupled Model Intercomparison Project (CMIP6). These data were used by Working Group I (WGI) in the AR6 and can be freely accessed in the Copernicus Climate Change Service (C3S) of the EU [91]. It should be noted that based on the new EU Strategy on Adaptation to Climate Change, the C3S is the main reference climate data source for climate change impact studies [37].

The most common approach for dealing with such datasets is the unweighted multi-model ensemble method (MME), in which each parameter of each model is treated equally and the forecast is retrieved by the simple mean or median of all participating models [92–94]. The use of MME has been proven to be superior, as it reduces the uncertainties related to the models' structure and parameterization [95] and is highly likely to express most aspects of climate change [96]. In the present study, the necessary hydrological model

forcing was retrieved using the unweighted multi-model ensemble mean of historical and future daily predicted time-series of precipitation, and maximum and minimum air temperature, of eight GCM models developed under CMIP6 (Table 3). The GCM models used in the present analysis were chosen based on the availability of the necessary meteorological variables for the hydrological model (precipitation and maximum and minimum air temperature), the experiment, and its spatial distribution over the study area.

Table 3. General Circulation Models used in the present study.

a/a	Model	Abbreviation	Resolution	Developer	Reference
1	Australian Community Climate and Earth System Simulator Climate Model Version 2	ACCESS-CM2	250 km	CSIRO [1]; ARCCSS [2]	[97]
2	Euro-Mediterranean Centre on Climate Change- Earth System Model version 2	CMCC-ESM2	100 km	CMCC [3]	[98,99]
3	Centre National de Recherches Météorologiques- Earth system model-second generation	CNRM-ESM2-1	250 km	CNRM [4]; CERFACS [5]	[100]
4	Earth Consortium 3 Carbon Cycle	EC-Earth3-CC	100 km	EC-Earth Consortium Europe: SMHI [6]; KNMI [7]; DMI [8]; AEMET [9]; Met Éireann; CNR [10]; BSC [11]; FMI [12] (core partners)	[101]
5	Institute for Numerical Mathematics Climate Model version 5, experiment 0	INM-CM5-0	100 km	INM [13]	[102]
6	Model for Interdisciplinary Research on Climate version 6	MIROC6	250 km	JAMSTEC [14]; AORI [15]; NIES [16]; R-CCS [17]	[103]
7	Meteorological Research Institute Earth System Model version 2.0	MRI-ESM2-0	100 km	MRI [18]	[104]
8	Norwegian Earth System Model version 2—Medium Resolution (atmosphere and land)/Medium Resolution (ocean and sea-ice)	NorESM2-MM	100 km	CICERO [19]; MET-Norway [20]; NERSC [21]; NILU [22]; UiB [23]; UiO [24]; UNI [25]	[105]

[1] Commonwealth Scientific and Industrial Research Organisation. [2] Australian Research Council Centre of Excellence for Climate System Science. [3] Centro Euro-Mediterraneo sui Cambiamenti Climatici. [4] Centre National de Recherches Météorologiques. [5] Centre Européen de Recherche et de Formation Avancée en Calcul Scientifique. [6] Sveriges meteorologiska och hydrologiska institut—Swedish Meteorological and Hydrological Institute. [7] Koninklijk Nederlands Meteorologisch Instituut- Royal Netherlands Meteorological Institute. [8] Danish Meteorological Institute. [9] Agencia Estatal de Meteorología. [10] Consiglio Nazionale delle Ricerche. [11] Barcelona Supercomputing Center. [12] Finnish Meteorological Institute. [13] Institute for Numerical Mathematics Russian Federation. [14] Japan Agency for Marine-Earth Science and Technology. [15] Atmosphere and Ocean Research Institute, The University of Tokyo. [16] National Institute for Environmental Studies. [17] RIKEN Center for Computational Science. [18] Meteorological Research Institute of Japan. [19] Center for International Climate and Environmental Research. [20] Norwegian Meteorological Institute. [21] Nansen Environmental and Remote Sensing Center. [22] Norwegian Institute for Air Research. [23] University of Bergen. [24] University of Oslo. [25] Uni Research.

Although the native CMIP6 resolutions are coarser than the study watershed, we minimized scale-related errors by selecting, for each GCM, the single grid cell whose historical time series best matched the available area-weighted average precipitation or air temperature records in terms of mean, seasonality, and interannual variability. This screening procedure ensures that the chosen grid point is climatologically representative of the watershed and aligns with the scope of the study to evaluate projected climate change signals rather than produce site-specific climate fields. It must be acknowledged that this does not replace formal downscaling, and our results should be interpreted as regional-scale signals rather than local-scale absolutes. We would also like to highlight that the currently available dataset of high-resolution (0.11° or ~12.5 km) EURO-CORDEX ensemble was driven by CMIP5 global climate models [106] and therefore could not be used in the present study.

Finally, it must be acknowledged that the objective of this study was to evaluate the hydrological response to the ensemble-mean climate change signal rather than to

characterize the uncertainty associated with individual GCM projections. Therefore, the bias-corrected outputs of the GCMs were averaged prior to driving the hydrological model, producing a representative mean forcing. This approach reduces model-specific variability.

The lack of necessary climatological data (i.e., relative humidity, solar radiation and wind speed) precluded the use of the Penman–Monteith equation [107] for the estimation of daily reference evapotranspiration (ET). Therefore, ET was estimated using the temperature-based Hargreaves empirical approach [108], which is recommended only in cases of lack of other meteorological data, and is considered to provide satisfactory results with an error rate of 10–15% or 1 mm/d, whichever is higher [109] (Figure 3).

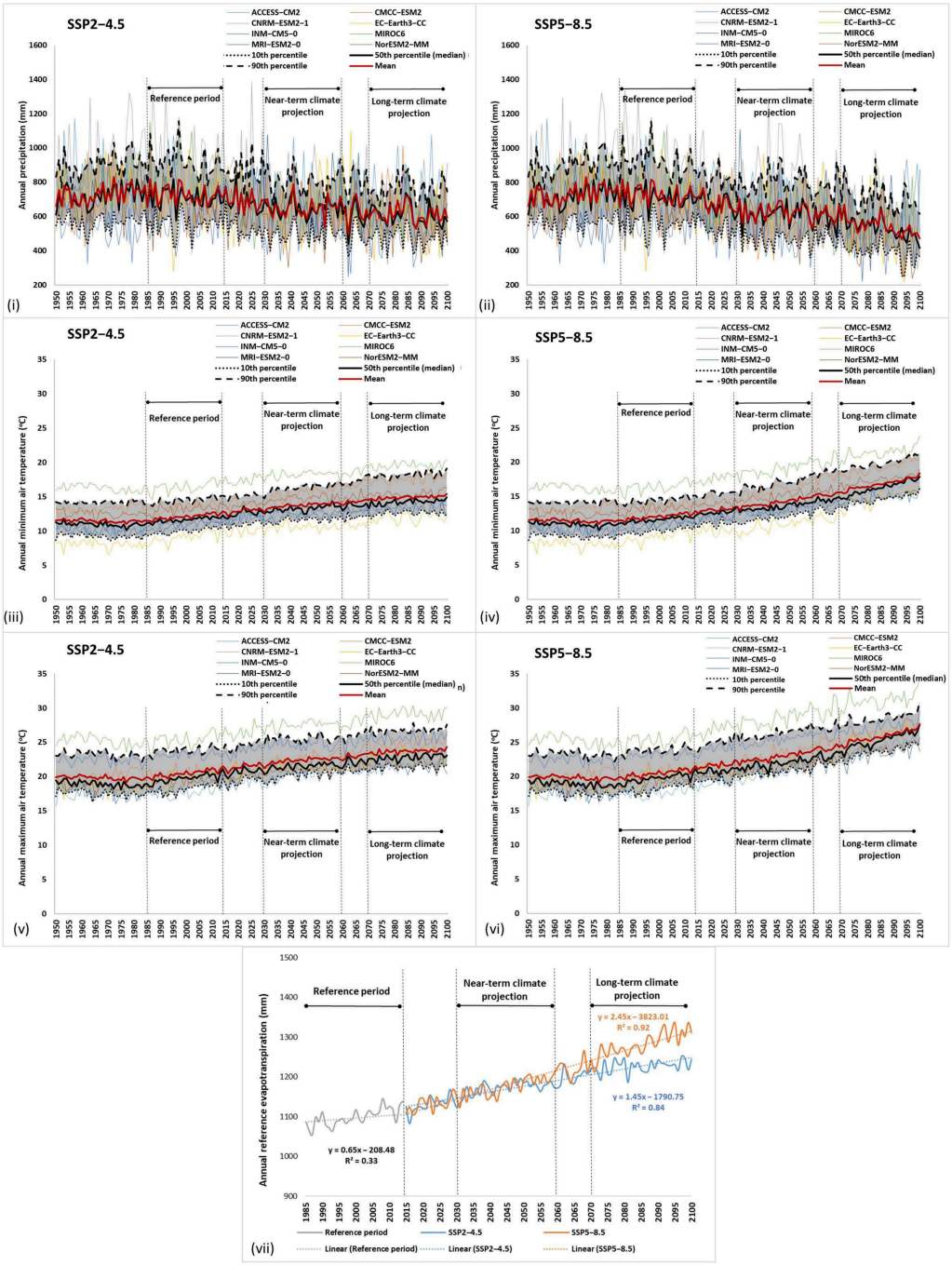

Figure 3. Predicted annual time series used in the hydrological modeling, (**i**,**ii**) annual precipitation, (**iii**,**iv**) annual minimum temperature, (**v**,**vi**) annual maximum temperature, for SSP2-4.5 and SSP5-8.5, respectively, and (**vii**) annual reference evapotranspiration, for both climate change scenarios examined.

Hydrometeorological and climatic studies focus on detecting anomalies, e.g., the variation of the predicted variables against a predefined reference period used as a baseline. The reference period length usually ranges between 20 and 50 years [110], while the World Health Organization (WHO) recommends a 30-year reference period for the calculation of the climate normals [111]. In the present study, the recommendation of WHO was adopted, and the period 1985–2014 was used as the reference period. Likewise, the anomalies were investigated against two future 30-year reference periods: a near-term period (2031–2060), and a long-term period (2071–2100).

The final time-series used in the present study (Spercheios river basin) and their main statistical characteristics are presented in Figure 3 and Table 4.

Table 4. Statistical characteristics of the climatological dataset used as forcing in hydrological modeling of Spercheios river basin for all climate change scenarios applied.

Parameter	Climate Change Scenario	Period	Minimum	Maximum	Mean		Median	1st Quartile	3rd Quartile
Precipitation (mm)	SSP2-4.5	Reference period	652	817	728		721	694	770
Average temperature (°C)	SSP2-4.5	Reference period	15.4	17.0	16.3		16.3	16.0	16.5
Reference evapotranspiration (mm)	SSP2-4.5	Reference period	1054	1145	1098		1095	1085	1114
Precipitation (mm)	SSP5-8.5	Reference period	652	817	728		721	694	770
Average temperature (°C)	SSP5-8.5	Reference period	15.4	17.0	16.3		16.3	16.0	16.5
Reference evapotranspiration (mm)	SSP5-8.5	Reference period	1054	1145	1098		1095	1085	1114
Precipitation (mm)	SSP2-4.5	Near-term	534	788	651	−11%	657	624	673
Average temperature (°C)	SSP2-4.5	Near-term	17.4	18.5	18.1	11%	18.1	17.9	18.3
Reference evapotranspiration (mm)	SSP2-4.5	Near-term	1134	1195	1172	7%	1175	1164	1181
Precipitation (mm)	SSP5-8.5	Near-term	533	703	629	−14%	633	609	671
Average temperature (°C)	SSP5-8.5	Near-term	17.3	19.7	18.5	14%	18.5	18.1	19.0
Reference evapotranspiration (mm)	SSP5-8.5	Near-term	1141	1241	1195	9%	1192	1183	1213
Precipitation (mm)	SSP2-4.5	Long-term	527	723	616	−18%	612	590	645
Average temperature (°C)	SSP2-4.5	Long-term	18.8	19.6	19.3	16%	19.3	19.2	19.5
Reference evapotranspiration (mm)	SSP2-4.5	Long-term	1185	1251	1226	10%	1229	1216	1240
Precipitation (mm)	SSP5-8.5	Long-term	466	671	543	−34%	536	508	573
Average temperature (°C)	SSP5-8.5	Long-term	19.8	22.8	21.4	24%	21.3	20.9	21.9
Reference evapotranspiration (mm)	SSP5-8.5	Long-term	1227	1380	1316	17%	1310	1295	1338

2.3. Evaluation of Hydrometeorological Extremes and Climatic Pressures

A variety of indicators have been proposed by the scientific community to accommodate the detection of extreme hydrometeorological and climate events. Each indicator usually focuses on a different aspect of the drought parameters, such as the duration, the severity, and the underlying mechanism [112,113]. In order to identify the climate change-related hydrometeorological extremes, and drought in particular, and climate-related pressures, the Standardized Precipitation Index (SPI) [114] was employed. This index has often been successfully used for climate impact studies and hydrometeorological drought analysis [113]. In SPI, precipitation data are fitted in a gamma distribution, providing information regarding drought duration and frequency. Likewise, the Standardized Precipitation Evapotranspiration Index (SPEI) [115] has also been developed to include the temperature component and has been proposed for use in climate change impact assessments to study model output under various future scenarios [112]. The SPI has been recommended by the WHO [116] to be used in drought research, while the European Drought Observatories (EDO) of the Copernicus Emergency Management Service (CEMS) and Global Drought Observatory (GDO) use both the SPI and the SPEI for similar studies [117,118]. In both indices, values lower than −1 indicate drought, and can be calculated for various timescales, usually 3, 6, 12, 24 and 48 months in relation to a reference period. In the present study the SPI-3 and SPEI-3 indicators were employed to investigate meteorological drought, while SPI-12 and SPEI-12 indicators were used to monitor hydrological

drought and impacts [112,116–118]. The SPI and SPEI calculations were performed in R v.4.6.0 software [119] using the "SPEI" package [120] (Equations (1) and (2) [121]).

$$SPI = \Phi^{-1}[F_{Gamma}(P)], \quad (1)$$

where Φ^{-1} is the quantile function of the standard normal distribution, P the accumulated precipitation over a chosen time scale (e.g., 3, 6, 12, or 24 months), and F_{Gamma} is the two-parameter Gamma distribution, fitted to the precipitation data.

$$SPEI = \Phi^{-1}[F_{Log\text{-}Logistic}(D)], \quad (2)$$

where Φ^{-1} is the quantile function of the standard normal distribution, D the climatic water balance, $D = P - PET$ (precipitation P minus potential evapotranspiration PET), and $F_{Log\text{-}Logistic}(D)$ the three-parameter log-logistic distribution, fitted to the climatic water balance.

The gamma distribution (SPI) and the log-logistic distribution (SPEI) were fitted using the historical reference period (1985–2014). The fitted distribution parameters were subsequently applied to the complete time series to obtain standardized indices for both the historical and future periods (2031–2060 and 2071–2100). No recalibration was performed for the future periods, thereby preserving the climatic shift relative to the historical baseline.

The precipitation-based indices mainly identify the drought-forcing mechanisms, the hydrological droughts and the watershed response to hydrometeorological factors. Climatic pressures can also be studied using low-flow standardized indicators, or boundaries and thresholds, so as to define periods of river flow deficits [19,122]. SPI-12 and SPEI-12 were included in the analysis because they provide information on persistent climatic water deficits, are widely applied in hydrological drought assessments, and constitute key indicators in operational drought monitoring and early warning systems. Complementarily, hydrological drought conditions were further evaluated using discharge-based low-flow indicators, ensuring that both climatic forcing and hydrological response were considered. Therefore, in the present study, the indicator of the number of days below low-flow boundaries per year was used, and the low-flow boundaries between moderate- and good-quality status concerning low-flow river discharge for each Mediterranean Geographical Intercalibration Group river type [123] were also employed. These low-flow boundaries were defined in a previous study to support the implementation of the WFD [45]. The boundary between moderate- and good-quality status is fundamental in meeting the objectives concerning the water quality status of aquatic systems set by WFD, as a status below moderate indicates the need for action and PoM implementation [29,33].

The number of days in the year when the river discharge is below a given threshold is a commonly used indicator also proposed by, among others, the Joint Research Centre (JRC) for the study of anthropogenic pressures on surface waterbodies of Europe [124,125]. The analysis was performed on the existing monitoring network of the study area established to meet the obligations arising from WFD regarding reporting the water status of surface waterbodies [46]. The WFD compliance monitoring of rivers aims to support the River Basin Management Plans (RBMPs) reporting and climate change adaptation assessment [33]. In Greece, the monitoring of rivers is being implemented by the Institute of Marine Biological Resources and Inland Waters of Hellenic Centre for Marine Research (HCMR-IMBRIW) under the supervision of the Special Secretariat for Water of Ministry of Environment and Energy of Greece [46]. In the Spercheios river basin, the river monitoring network comprises 11 sampling points (Figure 2, Table 5).

Table 5. Sampling points, part of the National Monitoring Network of Greece for the implementation of WFD in Spercheios river basin.

a/a	R-M Type	Site Name	Latitude (°)	Longitude (°)	EU Site Code	Surface Waterbody Code
1	R-M3	ALAMANA	22.322052	38.896862	EL0718R000200061N050	EL0718R000200061N
2	R-M5	DAMASTA	22.467008	38.803304	EL0718R000202051N050	EL0718R000202051N
3	R-M3	ELKE	22.494791	38.813325	EL0718R000200050N050	EL0718R000200050N
4	R-M5	FTERI	22.060637	38.929393	EL0718R000200064N100	EL0718R000200064N
5	R-M1	GORGO_DW	22.406432	38.841195	EL0718R000206059N050	EL0718R000206059N
6	R-M4	KRITHAR	22.232253	38.865970	EL0718R000208062N050	EL0718R000208062N
7	R-M2	MAKRI	22.159439	38.937886	EL0718R000200064N150	EL0718R000200064N
8	R-M2	T_LAM	22.479187	38.871144	EL0718R000204054A050	EL0718R000204054A
9	R-M3	T_SPER	22.475753	38.857622	EL0718R000204057A050	EL0718R000204057A
10	R-M5	VISTRITSA_DW	22.192827	38.908791	EL0718R000900079N050	EL0718R000900079N
11	R-M2	VISTRITSA_UP	22.085697	38.830404	EL0718R000904082N050	EL0718R000904082N

The impact of climate change on the study area was assessed using the number of days below low-flow boundary discharge anomalies at the monitoring network, e.g., the variation in the predicted variables against a predefined reference period used as a baseline. In the present study, the WHO recommendation was again adopted, and the period 1985–2014 was used as the reference period. Likewise, the number of days below low-flow boundary discharge anomalies was investigated against two 30-year future reference periods: a near-term period (2031–2060) and a long-term period (2071–2100).

Additionally, a trend analysis of the number of days below low-flow boundary discharge anomalies was performed for each monitoring station and for near- and long-term periods, to address serial dependence and multiple testing. Serial dependence was assessed by computing the Lag-1 autocorrelation coefficient (r_1) and testing its significance at $\alpha = 0.05$ using the approximation of Anderson [126]. In cases without significant r_1, the rank-based, non-parametric Mann–Kendall (MK) test [127,128] was applied, which is recommended by the WHO for hydrological and extreme event trend analysis [129]. The variance-corrected MK test proposed by Hamed and Rao (1998) [130] was applied in cases of significant r_1, which adjusts the test variance using an effective sample size to account for persistence. The trend slope was calculated using the Sen's slope (SS) estimator at 95% confidence intervals (CIs) [131]. To control the family-wise false positive rate arising from multiple parallel tests, we applied the Benjamini–Hochberg false discovery rate (FDR) procedure at $q = 0.05$ [132]. All reported significance levels reflect FDR-adjusted q-values rather than raw *p*-values. Operational significance was assessed using a ± 0.5 days/year threshold based on expert judgement, with trends classified as operationally significant only when the 95% CI fell entirely outside this range. Likewise, a trend analysis was performed on the climatological time-series used as forcing to the hydrological model for comparison. The trend analysis was performed in R v.4.6.0 software [119] using "trend" [133] and "Kendall" [134] packages.

Finally, in order to propose evidence-based PoMs, a water management program was adopted and applied based on the analysis described above, and evaluated concerning its effectiveness (Section 3.3).

3. Results

3.1. Hydrometeorological Extremes—Droughts

Based on the fluctuations in SPI-3 and SPEI-3 values in the Spercheios river basin, in the historical period, meteorological drought incidences (e.g., SPI-3 or SPEI-3 lower than

−1 [112]) were sparse. Additionally, these indices increased profoundly in near-term and long-term periods, in both climate change scenarios examined. More specifically, SPI-3 increased from 20 incidences in the historical period to 72 near-term and 127 long-term for climate change scenario SSP2-4.5, and from 4 incidences in the historical period to 59 near-term and 194 long-term for climate change scenario SSP5-8.5 (Figure 4i,iii,v). Likewise, the probability density plots indicate a shift towards drier conditions in both climate change scenarios examined, in relation to the historical period. Especially in the case of SSP5-8.5, the peak was located in values lower than −1, indicating the prevalence of dry conditions and meteorological drought. The variability was lower in the long-term period in both climate change scenarios examined, in comparison to the historical period and the near-term period (Figure 5i,ii).

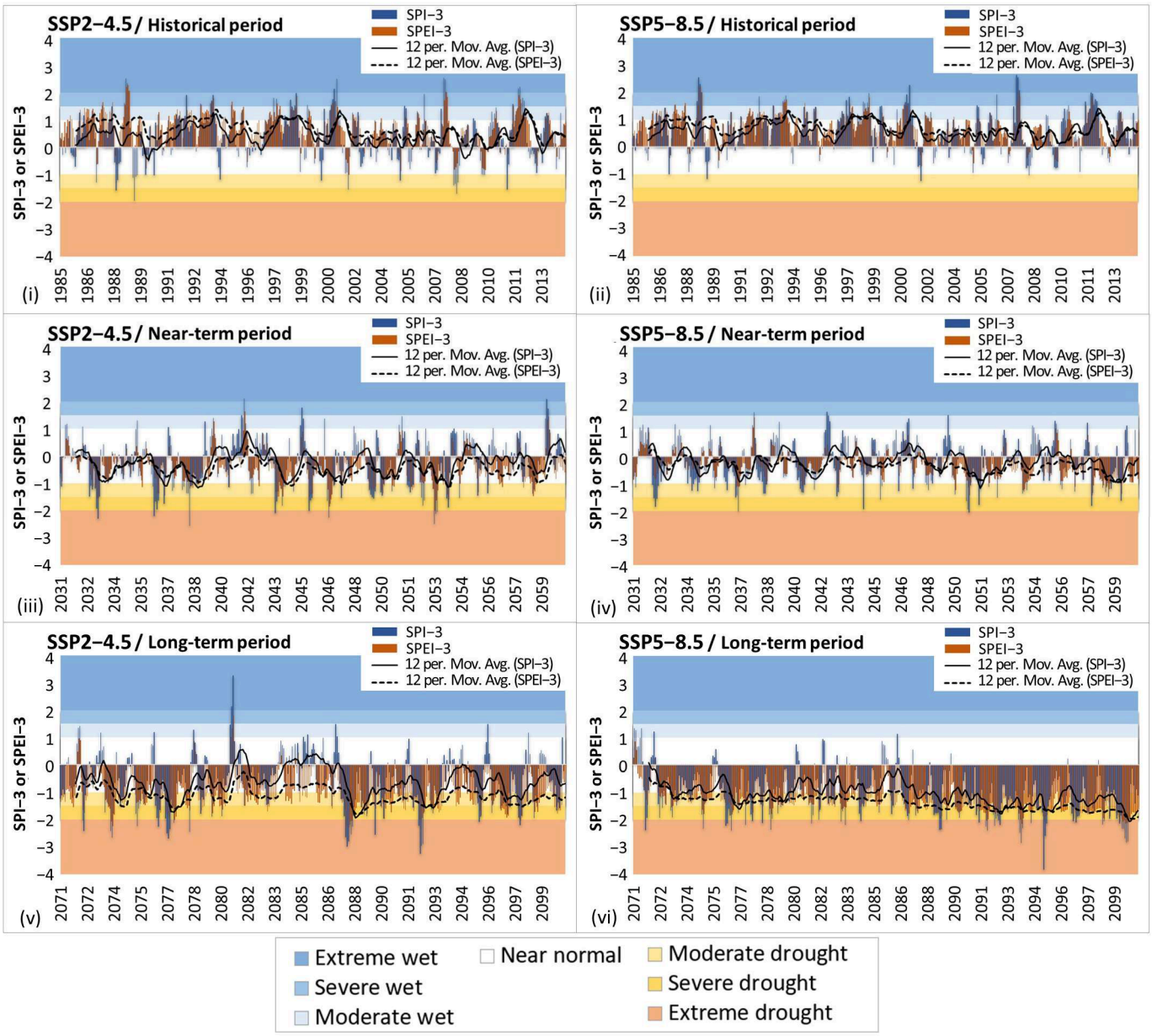

Figure 4. Temporal distribution of SPI-3 and SPEI-3 for SSP2-4.5 and SSP5-8.5 scenarios and (**i**,**ii**) historical period, (**iii**,**iv**) near-term period, and (**v**,**vi**) long-term period.

SPEI-3 increased from 1 incidence in the historical period to 66 near-term and 234 long-term for climate change scenario SSP2-4.5, and from 0 incidences in the historical period to

20 near-term and 308 long-term for climate change scenario SSP5-8.5 (Figure 4ii,iv,vi). The probability density plots indicate a shift towards drier conditions in both climate change scenarios examined. Again, the peak was located in values lower than −1 in the case of climate change SSP5-8.5, indicating the prevalence of dry conditions and meteorological drought, and likewise the variability was lower in the long-term period in both climate change scenarios examined (Figure 5iii,iv).

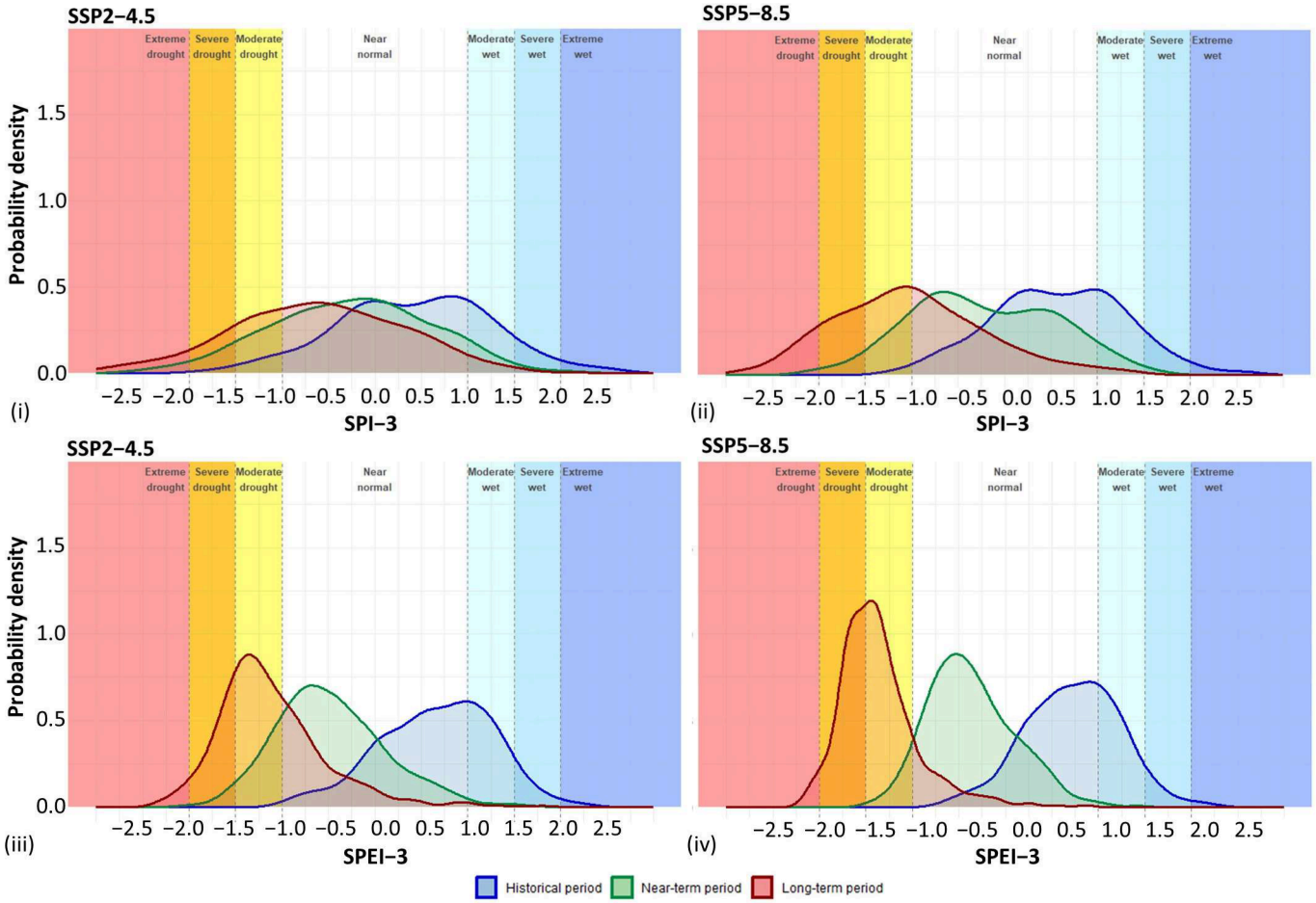

Figure 5. Probability density plots of SPI-3 (**i**,**ii**) and SPEI-3 (**iii**,**iv**) for climate change scenarios SSP2-4.5 and SSP5-8.5.

Likewise, in the historical period, hydrological drought incidences (e.g., SPI-12 or SPEI-12 lower than −1 [112]) were sparse, and increased profoundly in near-term and long-term periods, in both climate change scenarios examined. More specifically, SPI-12 increased from 0 incidences in the historical period to 86 near-term and 185 long-term for climate change scenario SSP2-4.5. For climate change scenario SSP5-8.5, SPI-12 increased from 0 incidences in the historical period to 46 near-term and 271 long-term (Figure 6i,iii,v). The probability density plots indicate a shift towards drier conditions in both climate change scenarios examined. In both cases, the curves are bimodal, and therefore the SPI-12 values are not evenly distributed and two subgroups of drought conditions can be identified. Again, the peak was located in values lower than −1 in the case of climate change scenario SSP5-8.5, indicating the prevalence of dry conditions and hydrological drought, and likewise the variability was lower in the long-term period in both climate change scenarios examined (Figure 7i,ii).

SPEI-12 increased from 0 incidence in the historical period to 37 near-term and 312 long-term, and from 0 incidences in the historical period to 1 near-term and

339 long-term for climate change scenario SSP5-8.5 (Figure 6ii,iv,vi). The probability density plots indicate a shift towards drier conditions in both climate change scenarios examined. In both cases, the curves are bimodal, and therefore the SPEI-12 values are not evenly distributed and two subgroups of drought conditions can be identified. Again, the peak was located in values lower than −1 in the case of climate change scenario SSP5-8.5, indicating the prevalence of dry conditions and hydrological drought, and likewise the variability was lower in the long-term period in both climate change scenarios examined (Figure 7iii,iv).

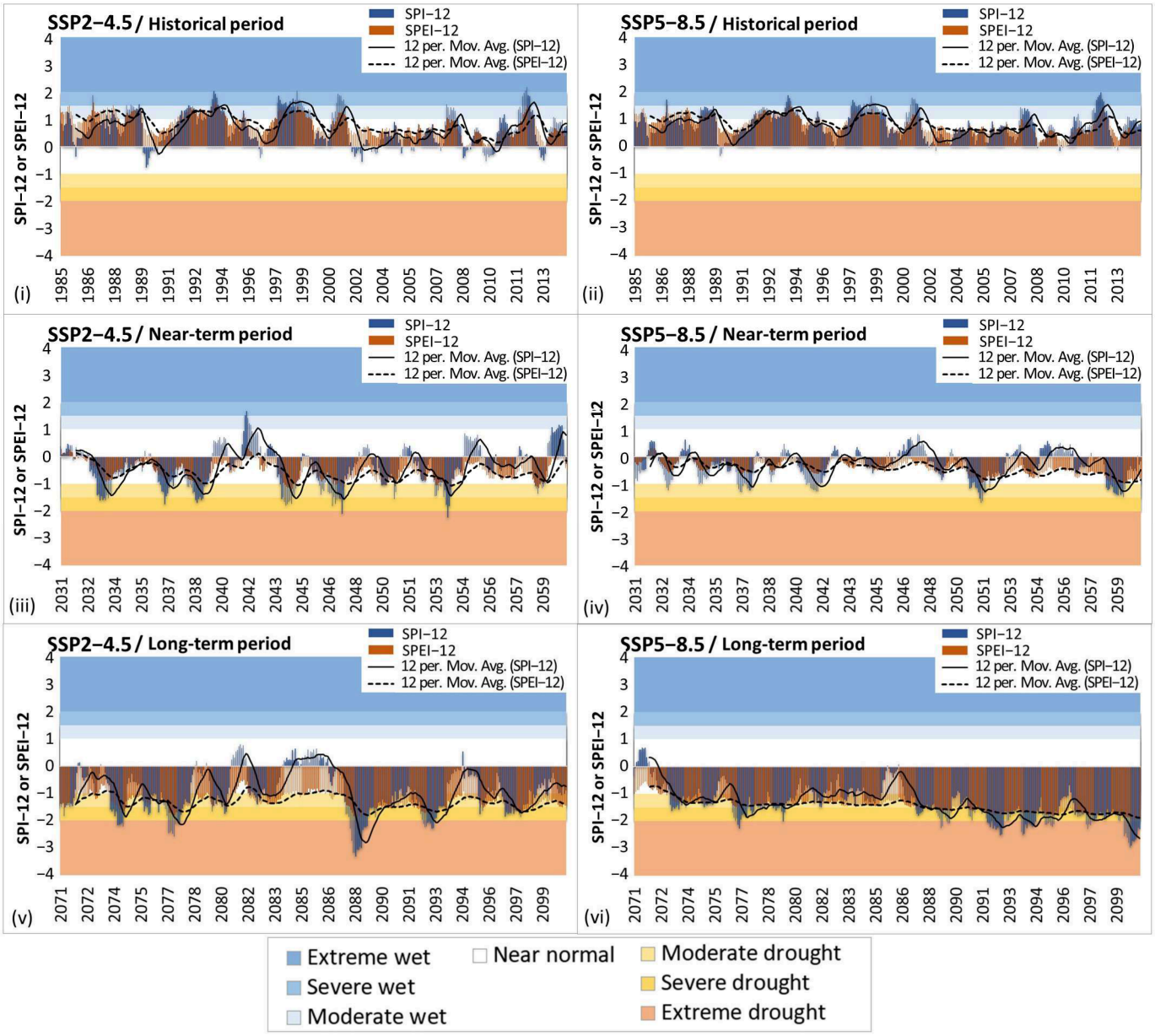

Figure 6. Temporal distribution of SPI-12 and SPEI-12 for SSP2-4.5 and SSP5-8.5 scenarios and (**i**,**ii**) historical period, (**iii**,**iv**) near-term period, and (**v**,**vi**) long-term period.

Overall, as expected, in the case of climate change scenario SSP5-8.5 and in the long-term period, the drought conditions were more profound in relation to the historical and the near-term periods. This can be attributed to the precipitation decrease, which reached 34% in climate change scenario SSP5-8.5 and for the long-term period, and to the simulta-

neous increase in air temperature up to 24% and consequence evapotranspiration increase up to 17% (Table 4).

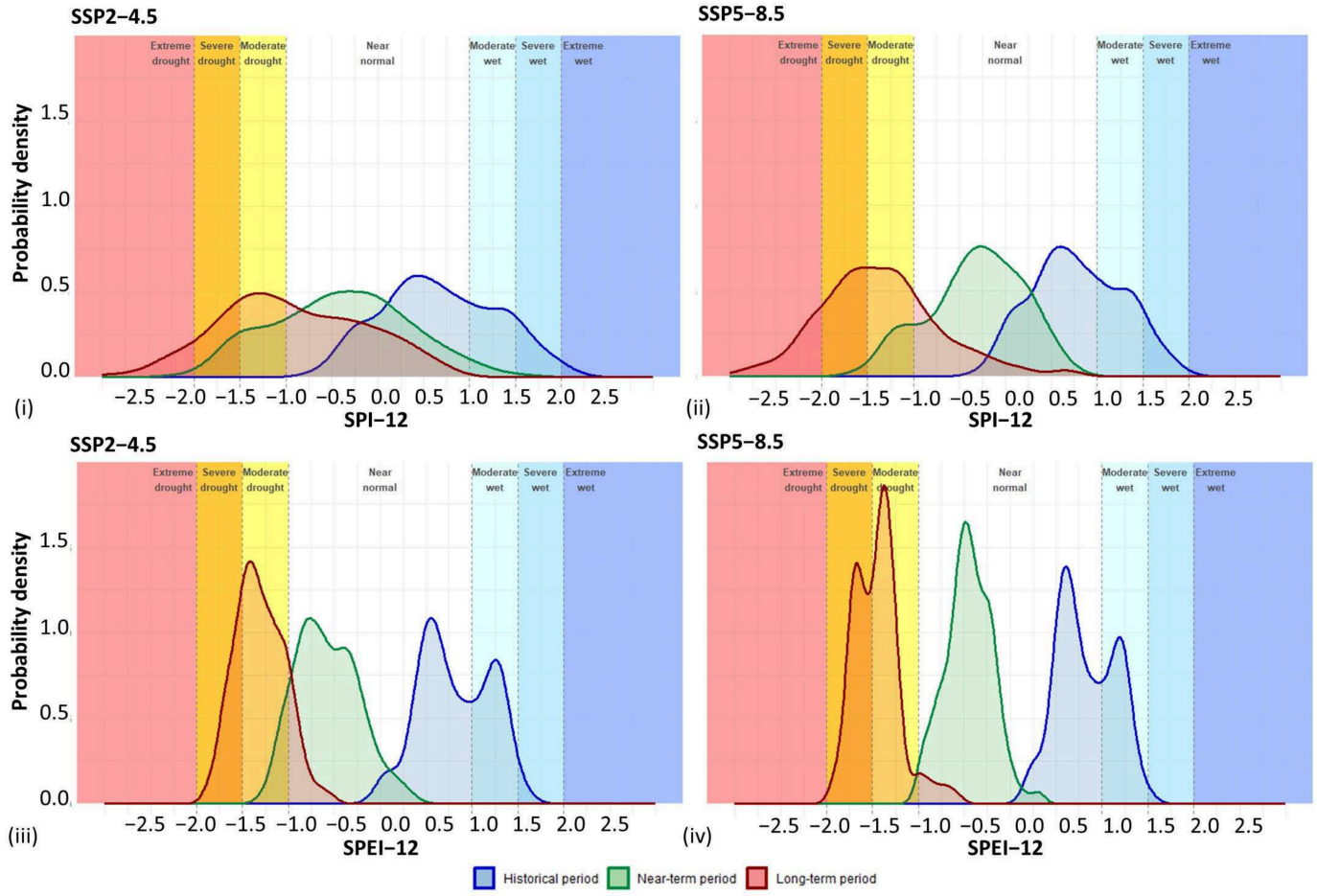

Figure 7. Probability density plots of SPI-12 (**i**,**ii**) and SPEI-12 (**iii**,**iv**) for climate change scenarios SSP2-4.5 and SSP5-8.5.

3.2. Climate Change Impacts

Based on the results, the average number of days below low-flow boundaries per year increased at all monitoring stations and for both near-term and long-term periods and both climate change scenarios examined. This increase was smaller for the near-term period and higher for the long-term periods for both climate change scenarios examined, as expected. The change was higher in all cases at the tributaries (Figure 8).

In all cases the impact of climate change on the running surface waterbodies was prominent. In the case of the SSP5-8.5 scenario, the number of days below low-flow boundaries per year anomalies was higher in comparison to the SSP2-4.5 scenario (higher positive anomalies). At all monitoring stations, the number of days below low-flow boundaries per year for the long-term period was higher than in the near-term period, as expected. The number of days below low-flow boundaries per year anomalies was higher upstream in the Spercheios river (monitoring station FTERI) and at the tributaries (Vistritsa or Inachos rivers—monitoring stations VISTRITSA_DW and VISTRITSA_UP; Kritharorrema river—monitoring station KRITHAR; Gorgopotamos river—monitoring station GORGO_DW; and Asopos river—monitoring station DAMASTA).

For the near-term period, the number of days below low-flow boundaries per year increased in both scenarios for all monitoring stations examined (except for the stations FTERI, GORGO_DW, T_LAM and VISTRITSA_DW), despite the corresponding increase

in precipitation for the same period, indicating the change in the distribution of rainfall throughout the year. For the long-term period, the number of days below low-flow boundaries per year increased at all monitoring stations and for both climate change scenarios examined, driven by the combined effects of the corresponding decrease in precipitation and enhanced evaporation demand. Based on the trend analysis performed, significant autocorrelation ($p < 0.05$) was detected primarily under the long-term period and SSP5-8.5 scenario. Of these cases examined, only ELKE and FTERI stations showed statistically significant trends, after FDR correction (ELKE: Sen's slope = +1.765 days/year; 95% CI: 0.857–2.714; q = 0.011; FTERI: +1.889 days/year; 95% CI: 0.682–2.565; q = 0.030), both under the SSP5-8.5 scenario and long-term period. All other trends had q > 0.05, including several with large point estimates but wide confidence intervals (e.g., T_LAM: +2.400 days/year; 95% CI: 1.273–3.500; q = 0.106). To distinguish statistical from operational significance, we applied a ±0.5 days/year threshold. Of the two statistically significant trends, both exceeded this threshold ('Statistically + operationally significant'). Four additional series were operationally significant but not statistically significant after FDR (DAMASTA, GORGO_DW, KRITHAR, T_LAM; all for the SSP5-8.5 scenario and long-term period), primarily due to wide confidence intervals (95% CI widths ranging 1.2–2.3 days/year) and reduced power from autocorrelation correction. No significant trends were detected under scenario SSP2-4.5 or in the near-term period (Tables 6 and 7, Figure 9).

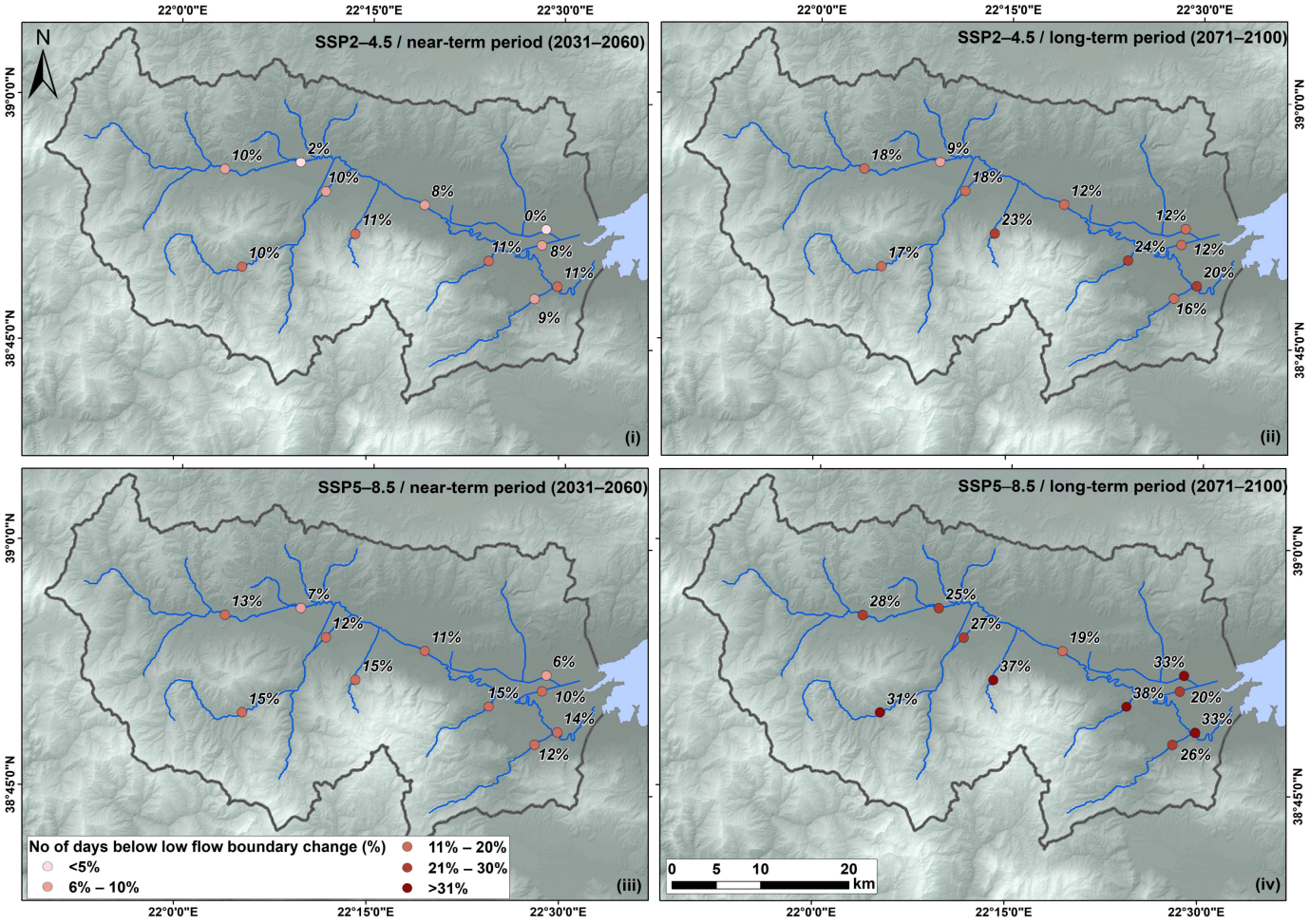

Figure 8. Predicted number of days below low-flow boundaries per year change for climate change scenario (**i**) SSP2-4.5 and the near-term period (2031–2060), (**ii**) SSP2-4.5 and long-term period (2071–2100), (**iii**) SSP5-8.5 and the near-term period (2031–2060), and (**iv**) SSP5-8.5 and long-term period (2071–2100), in relation to reference period (1985–2014).

Table 6. Mann–Kendall (MK) trend test results and Sen's slope (SS) for the climatological time-series of the climate change scenarios used as forcing in the hydrological model.

Monitoring Station	CCsc	Period	Autocorrelation Diagnostics				Mann–Kendall Test				Sen's Slope			FDR		Operational Significance	
			r1	r1_*p*	AC Sig	n_eff	MK Method	Tau	*p*	*p* corr	Sen Slope	lcl	ucl	q Value	Sign FDR	Oper Sig	Classification
P	SSP2-4.5	NT	−0.040	0.973	FALSE	30	Standard	0.122	0.354	0.354	0.730	−1.056	2.860	0.448	FALSE	FALSE	NS(FDR)
Tav	SSP2-4.5	NT	0.568	0.001	TRUE	14	HR	0.563	0.000	0.003	0.026	0.017	0.033	0.005	TRUE	FALSE	SS
ET	SSP2-4.5	NT	0.307	0.062	FALSE	30	Standard	0.324	0.013	0.013	0.857	0.231	1.474	0.018	TRUE	FALSE	SS
P	SSP5-8.5	NT	−0.021	0.944	FALSE	30	Standard	0.002	1.000	1.000	0.009	−2.130	2.521	1.000	FALSE	FALSE	NS(FDR)
Tav	SSP5-8.5	NT	0.677	0.000	TRUE	12.7	HR	0.779	0.000	0.000	0.059	0.048	0.070	0.001	TRUE	FALSE	SS
ET	SSP5-8.5	NT	0.492	0.004	TRUE	15.1	HR	0.614	0.000	0.001	2.502	1.776	3.158	0.002	TRUE	TRUE	S + OS
P	SSP2-4.5	LT	0.283	0.083	FALSE	30	Standard	−0.058	0.669	0.669	−0.233	−2.351	1.888	0.794	FALSE	FALSE	NS(FDR)
Tav	SSP2-4.5	LT	0.095	0.481	FALSE	30	Standard	0.402	0.002	0.002	0.017	0.007	0.025	0.005	TRUE	FALSE	SS
ET	SSP2-4.5	LT	−0.186	0.402	FALSE	30	Standard	0.205	0.116	0.116	0.550	−0.153	1.203	0.158	FALSE	FALSE	NS(FDR)
P	SSP5-8.5	LT	0.369	0.028	TRUE	17.3	HR	−0.476	0.000	0.005	−3.236	−4.680	−1.470	0.008	TRUE	TRUE	S + OS
Tav	SSP5-8.5	LT	0.781	0.000	TRUE	11.7	HR	0.853	0.000	0.000	0.076	0.068	0.088	0.000	TRUE	FALSE	SS
ET	SSP5-8.5	LT	0.606	0.001	TRUE	13.6	HR	0.706	0.000	0.000	3.205	2.510	4.178	0.001	TRUE	TRUE	S + OS

P: Precipitation (mm). Tav: Average temperature (°C). ET: Reference evapotranspiration (mm). CCsc: Climate change scenario. NT: Near-term. LT: Long-term. r1: Lag-1 autocorrelation coefficient. r1_*p*: *p*-value for autocorrelation test. AC Sig: Autocorrelation significance flag. n_eff: Effective sample size. HR: Hamed–Rao. Tau: Kendall's Tau statistic. *p*: Raw *p*-value (uncorrected). *p* corr: *p*-value after autocorrelation correction. lcl: Lower bound of 95% confidence interval. ucl: Upper bound of 95% confidence interval. q value: FDR-adjusted *p*-value (Benjamini–Hochberg). Sign FDR: FDR significance flag. Oper Sig: Exceeds your chosen threshold. Classification: Combined statistical + operational significance. NS: Not significant. SS: Statistically significant only. S + OS: Statistically + operationally significant.

Table 7. Mann–Kendall (MK) trend test results and Sen's slope (SS) for of the number of days below low flow boundaries per year anomalies, for the monitoring stations of Spercheios river basin.

Monitoring Station	CCsc	Period	Autocorrelation Diagnostics				Mann–Kendall Test				Sen's Slope			FDR		Operational Significance	
			r1	r1_*p*	AC Sig	n_eff	MK Method	Tau	*p*	*p* corr	Sen Slope	lcl	ucl	q Value	Sign FDR	Oper Sig	Class-ification
ALAMANA	SSP2-4.5	NT	0.063	0.597	FALSE	30	Standard	−0.169	0.199	0.199	−0.389	−1.000	0.250	0.470	FALSE	FALSE	NS(FDR)
	SSP2-4.5	LT	−0.114	0.659	FALSE	30	Standard	0.051	0.708	0.708	0.167	−0.643	1.000	0.840	FALSE	FALSE	NS(FDR)
	SSP5-8.5	NT	0.153	0.308	FALSE	30	Standard	−0.007	0.971	0.971	0.000	−0.600	0.533	0.994	FALSE	FALSE	NS(FDR)
	SSP5-8.5	LT	0.096	0.480	FALSE	30	Standard	0.289	0.028	0.028	0.571	0.056	1.095	0.117	FALSE	FALSE	NS(FDR)
DAMASTA	SSP2-4.5	NT	0.051	0.645	FALSE	30	Standard	−0.192	0.143	0.143	−0.444	−1.000	0.167	0.403	FALSE	FALSE	NS(FDR)
	SSP2-4.5	LT	0.043	0.675	FALSE	30	Standard	0.072	0.592	0.592	0.182	−0.500	0.706	0.762	FALSE	FALSE	NS(FDR)
	SSP5-8.5	NT	0.221	0.163	FALSE	30	Standard	−0.072	0.592	0.592	−0.160	−0.636	0.546	0.762	FALSE	FALSE	NS(FDR)
	SSP5-8.5	LT	0.552	0.001	TRUE	14.3	HR	0.470	0.000	0.012	1.167	0.500	1.765	0.089	FALSE	FALSE	NS(FDR)
ELKE	SSP2-4.5	NT	−0.005	0.876	FALSE	30	Standard	−0.116	0.382	0.382	−0.353	−1.000	0.571	0.678	FALSE	FALSE	NS(FDR)
	SSP2-4.5	LT	0.135	0.357	FALSE	30	Standard	0.127	0.335	0.335	0.364	−0.667	1.143	0.678	FALSE	FALSE	NS(FDR)
	SSP5-8.5	NT	0.247	0.125	FALSE	30	Standard	−0.049	0.721	0.721	−0.158	−0.857	0.667	0.840	FALSE	FALSE	NS(FDR)
	SSP5-8.5	LT	0.319	0.054	FALSE	30	Standard	0.451	0.001	0.001	1.765	0.857	2.714	0.011	TRUE	TRUE	S + OS
FTERI	SSP2-4.5	NT	0.114	0.420	FALSE	30	Standard	−0.081	0.544	0.544	−0.200	−1.000	0.571	0.762	FALSE	FALSE	NS(FDR)
	SSP2-4.5	LT	0.119	0.405	FALSE	30	Standard	0.081	0.544	0.544	0.318	−1.000	1.304	0.762	FALSE	FALSE	NS(FDR)
	SSP5-8.5	NT	0.218	0.169	FALSE	30	Standard	0.071	0.592	0.592	0.444	−0.769	1.444	0.762	FALSE	FALSE	NS(FDR)
	SSP5-8.5	LT	0.321	0.052	FALSE	30	Standard	0.403	0.002	0.002	1.889	0.682	2.565	0.030	TRUE	TRUE	S + OS
GORGO_DW	SSP2-4.5	NT	−0.140	0.560	FALSE	30	Standard	−0.150	0.253	0.253	−0.563	−1.458	0.400	0.570	FALSE	FALSE	NS(FDR)
	SSP2-4.5	LT	0.164	0.280	FALSE	30	Standard	0.187	0.153	0.153	1.036	−0.333	2.160	0.406	FALSE	FALSE	NS(FDR)
	SSP5-8.5	NT	−0.124	0.621	FALSE	30	Standard	0.035	0.803	0.803	0.182	−0.929	1.000	0.840	FALSE	FALSE	NS(FDR)
	SSP5-8.5	LT	0.565	0.001	TRUE	14.1	HR	0.412	0.002	0.029	2.100	1.208	3.316	0.117	FALSE	TRUE	NS(FDR)
KRITHAR	SSP2-4.5	NT	−0.046	0.945	FALSE	30	Standard	−0.097	0.464	0.464	−0.389	−1.217	0.600	0.762	FALSE	FALSE	NS(FDR)
	SSP2-4.5	LT	0.106	0.446	FALSE	30	Standard	0.136	0.301	0.301	0.546	−0.700	1.500	0.644	FALSE	FALSE	NS(FDR)
	SSP5-8.5	NT	0.219	0.167	FALSE	30	Standard	−0.039	0.775	0.775	−0.182	−1.000	0.857	0.840	FALSE	FALSE	NS(FDR)
	SSP5-8.5	LT	0.379	0.024	TRUE	17.1	HR	0.445	0.001	0.009	2.214	1.087	3.235	0.089	FALSE	TRUE	NS(FDR)

Table 7. *Cont.*

Monitoring Station	CCsc	Period	Autocorrelation Diagnostics				Mann–Kendall Test				Sen's Slope			FDR		Operational Significance	
			r1	r1_*p*	AC Sig	n_eff	MK Method	Tau	*p*	*p* corr	Sen Slope	lcl	ucl	q Value	Sign FDR	Oper Sig	Class-ification
MAKRI	SSP2-4.5	NT	0.173	0.258	FALSE	30	Standard	−0.311	0.018	0.018	−0.667	−1.214	−0.111	0.106	FALSE	FALSE	NS(FDR)
	SSP2-4.5	LT	0.015	0.793	FALSE	30	Standard	0.113	0.392	0.392	0.450	−0.600	1.353	0.678	FALSE	FALSE	NS(FDR)
	SSP5-8.5	NT	0.062	0.601	FALSE	30	Standard	−0.074	0.580	0.580	−0.200	−0.778	0.429	0.762	FALSE	FALSE	NS(FDR)
	SSP5-8.5	LT	0.406	0.016	TRUE	16.6	HR	0.351	0.007	0.043	1.421	0.385	2.250	0.162	FALSE	FALSE	NS(FDR)
T_LAM	SSP2-4.5	NT	0.050	0.648	FALSE	30	Standard	−0.250	0.056	0.056	−0.750	−1.474	0.000	0.194	FALSE	FALSE	NS(FDR)
	SSP2-4.5	LT	0.211	0.181	FALSE	30	Standard	0.240	0.066	0.066	1.158	−0.091	2.091	0.212	FALSE	FALSE	NS(FDR)
	SSP5-8.5	NT	−0.103	0.704	FALSE	30	Standard	0.035	0.803	0.803	0.091	−0.790	0.952	0.840	FALSE	FALSE	NS(FDR)
	SSP5-8.5	LT	0.535	0.002	TRUE	14.5	HR	0.432	0.001	0.020	2.400	1.273	3.500	0.106	FALSE	TRUE	NS(FDR)
T_SPER	SSP2-4.5	NT	0.079	0.539	FALSE	30	Standard	−0.119	0.372	0.372	−0.333	−1.000	0.286	0.678	FALSE	FALSE	NS(FDR)
	SSP2-4.5	LT	−0.007	0.884	FALSE	30	Standard	0.046	0.735	0.735	0.167	−0.750	0.889	0.840	FALSE	FALSE	NS(FDR)
	SSP5-8.5	NT	−0.028	0.974	FALSE	30	Standard	−0.123	0.353	0.353	−0.333	−0.857	0.333	0.678	FALSE	FALSE	NS(FDR)
	SSP5-8.5	LT	0.212	0.180	FALSE	30	Standard	0.301	0.021	0.021	0.818	0.154	1.444	0.106	FALSE	FALSE	NS(FDR)
VISTRI-TSA_DW	SSP2-4.5	NT	0.120	0.400	FALSE	30	Standard	0.078	0.556	0.556	0.313	−0.696	1.286	0.762	FALSE	FALSE	NS(FDR)
	SSP2-4.5	LT	0.219	0.167	FALSE	30	Standard	0.035	0.803	0.803	0.111	−0.941	1.571	0.840	FALSE	FALSE	NS(FDR)
	SSP5-8.5	NT	0.345	0.039	TRUE	17.8	HR	0.053	0.694	0.751	0.154	−0.905	1.500	0.840	FALSE	FALSE	NS(FDR)
	SSP5-8.5	LT	0.231	0.148	FALSE	30	Standard	0.330	0.012	0.012	1.000	0.125	1.900	0.089	FALSE	FALSE	NS(FDR)
VISTRI-TSA_UP	SSP2-4.5	NT	0.069	0.575	FALSE	30	Standard	−0.216	0.103	0.103	−0.333	−1.000	0.069	0.310	FALSE	FALSE	NS(FDR)
	SSP2-4.5	LT	−0.041	0.969	FALSE	30	Standard	0.002	1.000	1.000	0.000	−0.667	0.917	1.000	FALSE	FALSE	NS(FDR)
	SSP5-8.5	NT	0.034	0.714	FALSE	30	Standard	−0.075	0.579	0.579	−0.143	−0.826	0.455	0.762	FALSE	FALSE	NS(FDR)
	SSP5-8.5	LT	0.420	0.013	TRUE	16.3	HR	0.241	0.066	0.168	0.800	0.000	1.500	0.420	FALSE	FALSE	NS(FDR)

P: Precipitation (mm). Tav: Average temperature (°C). ET: Reference evapotranspiration (mm). CCsc: Climate change scenario. NT: Near-term. LT: Long-term. r1: Lag-1 autocorrelation coefficient. r1_*p*: *p*-value for autocorrelation test. AC Sig: Autocorrelation significance flag. n_eff: Effective sample size. HR: Hamed–Rao. Tau: Kendall's Tau statistic. *p*: Raw *p*-value (uncorrected). *p* corr: *p*-value after autocorrelation correction. lcl: Lower bound of 95% confidence interval. ucl: Upper bound of 95% confidence interval. q value: FDR-adjusted *p*-value (Benjamini–Hochberg). Sign FDR: FDR significance flag. Oper Sig: Exceeds your chosen threshold. Classification: Combined statistical + operational significance. NS: Not significant. SS: Statistically significant only. S + OS: Statistically + operationally significant.

Overall, the impact of climate change on the low flows of the hydrographic network of the study area was significant in the case of scenario SSP5-8.5 and for the long-term period, due to the corresponding decrease in precipitation. In all cases the number of days below low-flow boundaries per year increased, despite the fact that the number of days below low-flow boundaries per year trend decreased for the near-term period for both scenarios. This indicates the impact of climate change on the hydrological regime and low flows in particular of the rivers of the study area. Based on the results, the impact of climate change is more prominent upstream and at the tributaries, indicating the susceptibility of smaller rivers to climate change (R-M1, R-M4 or R-M5 river types).

3.3. Water Management Plan

Based on the recent 2nd Update of the RBMPs of Greece, the agricultural sector is the dominant consumer of freshwater in the Spercheios river basin, reaching 94% of the total water withdrawals. Due to abstractions for irrigation, some downstream surface waterbodies fail to achieve good ecological status [135]. For this reason, a water management plan consisting of a 25% reduction in irrigation demand and water withdrawals from groundwater reservoirs through point abstractions points—boreholes—was adopted for the area was adopted. This water management plan was applied to the hydrological model of the Spercheios river basin for both climate change scenarios examined in the present study, so as to test its effect on the hydrological regime and the low-flow discharges in particular, and eventually its effectiveness. The proposed 25% reduction in irrigation demand and water

withdrawals from groundwater is a realistic and feasible management plan, that based on the literature can be applied without significantly affecting the quantity and quality of the harvested yield of cultivations found at the demonstration site [136]. Additionally, it should be noted that in the present study, we avoided using different water management plans simultaneously, due to the arising complexity, which increases uncertainties during hydrological simulation and the interpretation of results [21].

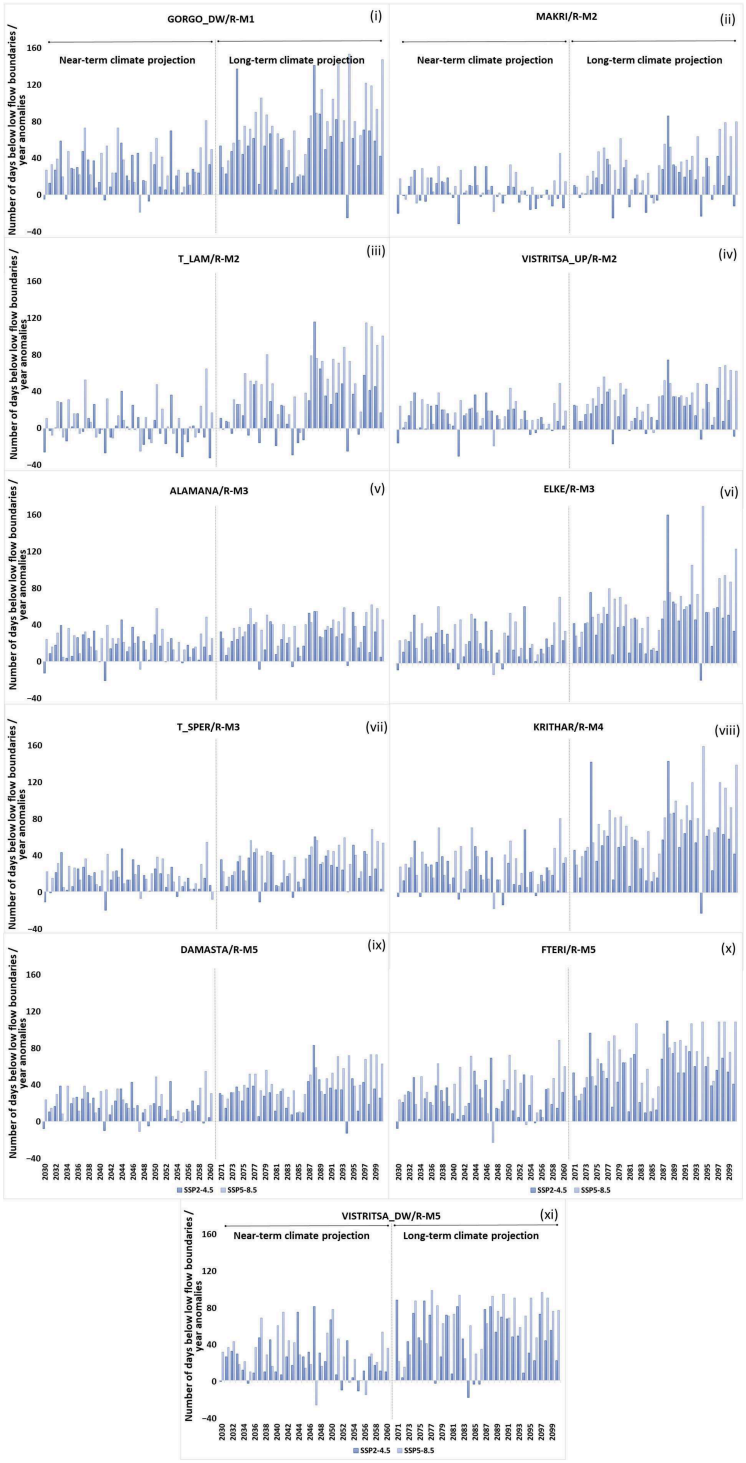

Figure 9. Anomalies of the number of days below low-flow boundaries per year (reference period 1985–2014), for monitoring stations (**i**) GORGO_DW, (**ii**) MAKRI, (**iii**) T_LAM, (**iv**) VISTRITSA_UP, (**v**) ALAMANA, (**vi**) ELKE, (**vii**) T_SPER, (**viii**) KRITHAR, (**ix**) DAMASTA, (**x**) FTERI, and (**xi**) VISTRITSA_DW.

Based on the results (Figure 10), a 25% reduction in irrigation demand and groundwater withdrawals would lead to a small reduction in the number of days below the low-flow boundary downstream, where the majority of water abstraction points are located (Figure 2). Upstream, no reduction in the number of days below the low-flow boundary was stated. This is not surprising, as upstream irrigation demands and water abstractions are limited. Overall, although the effect of the water management plan on the water resources was notable, it was not significant, and reached only a maximum of 3% reduction (site T_SPER for climate change scenario SSP5-8.5, long-term period). Likewise, a small reduction was stated at the monitoring sites ALAMANA, DAMASTA, ELKE, MAKRI and VISTRITSA_DW for climate change scenario SSP5-8.5 and the long-term period.

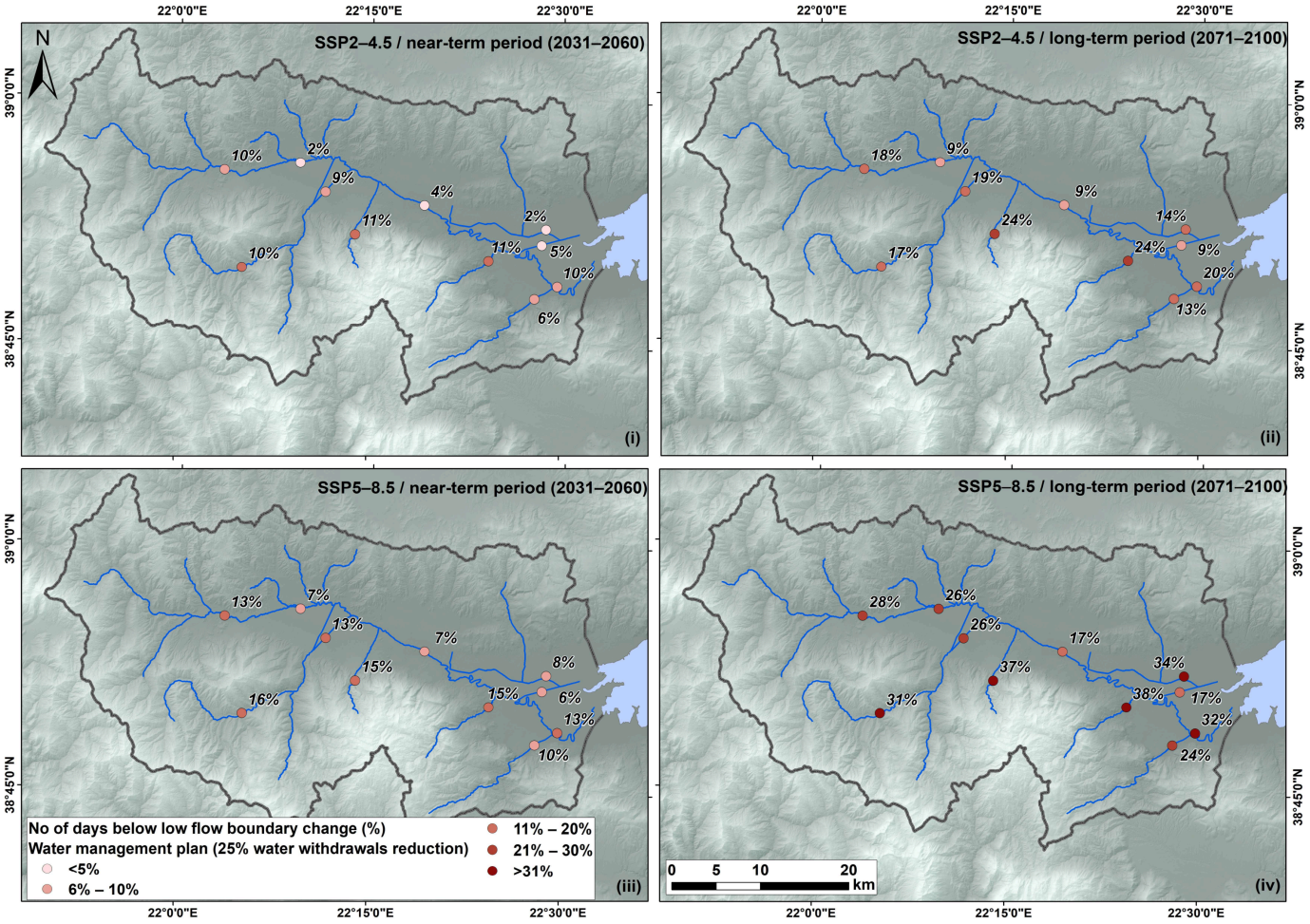

Figure 10. Predicted number of days below low-flow boundaries per year change, for the water management plan applied (25% water withdrawal reduction), and for climate change scenario (**i**) SSP2-4.5 and the near-term period (2031–2060), (**ii**) SSP2-4.5 and long-term period (2071–2100), (**iii**) SSP5-8.5 and the near-term period (2031–2060), and (**iv**) SSP5-8.5 and long-term period (2071–2100), in relation to reference period (1985–2014).

4. Discussion

The WFD was adopted more than 25 years ago to provide a legal tool for freshwater protection and restoration. Nevertheless, Europe's growing water crises indicate the insufficient implementation of the PoMs of the RBMPs, but also the inability to incorporate hydrometeorological extremes and climate change-related measures [137]. Human-caused climate change is turning Europe into the fastest-warming continent. Consequently, climate change is expected to exacerbate pressures such as pollution, increased water demand, poor

water management practices, land use and hydromorphological changes, and urbanization put on freshwater, and to accelerate Europe's existing water risk and crises [138]. Effective climate-resilient water management in the context of WRS has been recently promoted. This concept focuses on the ability of the system to maintain essential functions while adapting to new climate-induced conditions, and integrates adaptive strategies, technologies, and policies to ensure water security despite climate change [139]. Key approaches include managed aquifer recharge, watershed restoration, and artificial intelligence (AI)-driven irrigation [36]. WRS also highlights the need for Drought Management Plans (DMPs) and the development of water scarcity indicators [36], along with RBMPs or integrally, to manage water scarcity and drought risks more effectively [33].

The application of this framework to the demonstration site may be constrained by the deduced low-flow performance confined to two monitoring stations (Gorgopotamos and Komma), which may reflect local observational limitations that are not fully represented by the model. Consequently, uncertainty in the simulated number of days below the discharge threshold is expected to be greater at these locations, whereas low-flow performance at the remaining stations supports confidence in the broader regional assessment. Likewise, the use of the Hargreaves empirical method for the daily reference evapotranspiration estimation introduces uncertainty into both the hydrological simulations and the SPEI calculations. Alternative ET formulations, such as Penman–Monteith, may produce different estimates of evaporative demand under future climate conditions because they explicitly account for radiation, humidity, and wind speed. Evaluating the sensitivity of the results to the ET formulation and propagating ET-related uncertainty through the modelling framework represents an important direction for future research but is beyond the scope of the present study. It is also important to acknowledge that uncertainties arising from GCM predictions, hydrological model parameterization, and input data sets are inherent to climate impact estimates. Although a formal quantitative uncertainty analysis (such as Monte Carlo simulations) was beyond the scope of this regional risk assessment framework, these structural limitations suggest that our hydroclimatic results should be interpreted as indicative regional stress-tests and trends rather than precise, deterministic predictions. It is worth noting that hydrological modeling introduces uncertainties, particularly regarding groundwater–surface water interactions, baseflow and low-flow persistence. Future applications of the framework could benefit from conducting sensitivity analyses to better define characteristic parameters of these parameters. Finally, it is recognized that exploring more complex water management scenarios, such as varying magnitudes of reduction in irrigation demand and groundwater withdrawals, environmental flow augmentation, or cropping pattern adjustment, could provide a more detailed description of the system's response to the anthropogenic activities. However, simulating these complex scenarios would introduce multiple levels of parameter uncertainties, the analysis and interpretation of which are beyond the primary objective of this study and, therefore, their integrated implementation represents critical pathways for future research. Therefore, only a simple, realistic and feasible scenario was examined, which served as a clearly defined trend indicator and a unit-change sensitivity test, rather than an absolute forecast, allowing a more accurate identification of the climate change signal without the confounding effects of the contribution of multiple factors.

Climate change has been identified as a significant driver that may have an environmental effect, and adaptation to climate change has been identified as a key type measure (KTM24) during WFD reporting [140]. Although, during the recent 3rd RBMPs, most member states assessed the effect of climate change on waterbodies, the linkage between this driver and the corresponding mitigation measures was mostly unsuccessful [137]. In the recent 3rd RBMPs, specific basic and supplementary measures for climate change

adaptation were linked to the key type measures introduced to facilitate the PoMs reporting under the WFD [140]. These proposed measures, which are also related to those proposed by the NCCAS of Greece, are not supported by a quantitative analysis. The proposed framework incorporated hydrological modelling, future projections of precipitation and air temperature, low-flow river flow boundaries to support river health established in previous study, and quantitative statistical analysis.

Additionally, the proposed framework was supported by the quantitative assessment of the most important PoM proposed, e.g., the reduction in groundwater withdrawals and irrigation demands. Our study showed that although irrigation has been identified as a major factor intensifying hydrological droughts in Southern Europe [141], in the Spercheios river basin, climatic factors affect drought frequency more profoundly than human water use. Based on these results, the adoption of a single action may not be sufficient. Therefore, apart from the dominant measure proposed concerning irrigation demands and groundwater abstraction reduction, additional actions can be proposed for climate change mitigation. Using the present study area as a demonstration site, comprehensive measures, which were partially identified during the 3rd RBMP [142], and an operational framework and adaptation actions for the mitigation of the hydrometeorological and climate change pressures in rivers of Greece are proposed (Table 8).

Table 8. PoMs and adaptation actions proposed for hydrometeorological and climate change pressure mitigation.

Indicator	Driver	Response	Threshold	Action	Measure	WFD Article 11 Measure
SPI-3/SPEI-3	meteorological drought hydrometeorological pressures	soil moisture deficit, high-to-medium-term drought	<−1.0	Drought warning (restrictions triggered)	- volumetric pricing of water abstraction with drought surcharge	11.3.c
			<−1.5 for three months		- drought emergency plan development	11.3.c
					- preparation/update of the Water Supply Masterplans	11.3.c
SPI-12/SPEI-12	hydrological drought climatic pressures	water scarcity, groundwater storage deficit, river low flow/baseflow interruption, drought propagation	<−1.0	Permanent measures	- abstraction license reduction	11.3.e
					- stricter consent limits during low-flow periods (dynamic permits)	11.3.c
			<−1.5 for 2 consecutive years		- industrial water/wastewater treatment plant recycling mandates	11.3.c
					- shift to drought-resilient crops in cooperation with the Common Agricultural Policy (CAP)	11.3.c
Low flow days anomalies	hydrological drought hydrometeorological pressures	hydrological regime alteration, river low flow/baseflow interruption	number of days below low-flow boundaries per year [45]		- implementation of more efficient irrigation methods to reduce usage	11.3.c
			+30 more low-flow days/year in relation to the reference period (e.g., 1985–2014)		- environmental flow enforcement	11.3.i
					- barrier removal/river restoration	11.3.i
Discharge anomalies	hydrological drought climatic pressures	hydrological regime alteration	<−30% during low-flow season in relation to the reference period (e.g., 1985–2014)		- off-stream storage constructions (NbS)	11.3.f
					- Restore floodplains and wetlands to retain water (NbS)	11.3.f
					- Re-meander channels to increase residence time (NbS)	11.3.f

11.3.c: Basic measures to promote an efficient and sustainable water use; 11.3.e: Basic measures regarding controls over abstractions, impoundment of fresh surface water, registration and monitoring for all abstraction activities and revision of existing water abstraction permits; 11.3.f: Basic measures regarding the artificial recharge or augmentation of groundwater bodies; 11.3.i: Basic measures on hydromorphology.

More specifically, Table 8 presents a multi-scalar management framework that distinguishes between meteorological (SPI-3 or SPEI-3) and hydrological (SPI-12/SPEI-

12, low-flow days, discharge anomalies) drought drivers. This framework allows a comparative analysis of propagation dynamics and response thresholds. The SPI-3 or SPEI-3 threshold of <−1.0 captures high-to-medium-term soil moisture deficits, triggering volumetric pricing as a demand-side economic tool. A sustained breach of values < −1.5 over three months activates preparatory emergency planning, which represents an empirical threshold that researchers could validate against historical drought impacts on water supply reliability. For hydrological drought, the framework introduces a permanent versus conditional action logic. More specifically, an SPI-12 or SPEI-12 value below −1.0 mandates permanent abstraction license reductions, whereas two consecutive years below −1.5 triggers dynamic permitting, industrial recycling mandates, and land-use shifts under the Common Agricultural Policy, offering a testable hypothesis about whether multi-annual memory improves drought resilience relative to single-year thresholds. Additional indicators (anomalies in low-flow days and discharge anomalies) trigger environmental flow enforcement, barrier removal, and nature-based solutions (NbSs) such as floodplain restoration and channel re-meandering. Overall, the table effectively operationalizes drought monitoring by linking escalating biophysical thresholds to progressive, context-specific management actions.

This operational scheme, which is based on quantitative thresholds that trigger actions and measures for adaptation, can be used by decision-makers and stakeholders as guidelines for mitigation actions; nevertheless, adjustments to the local conditions and needs may be necessary. Likewise, the thresholds proposed for triggering action have been based on the literature and may be subjected to modifications to meet local needs. For example, a 20% reduction in low-flow streamflow can compromise a river's health and could be considered a threshold for trigger action [143,144], while 30% of the average flow between June and August is the minimum environmental flow defined based on the Greek legislation [145]. Nevertheless, further investigation is essential for the site-specific definition of a threshold for triggering action. Finally, new technologies, AI tools, early-warning systems, and nature-based solutions (NbSs) are emerging solutions to climate change adaptation and river health protection [146–148].

5. Conclusions

The health and ecological integrity of Greek rivers are affected by hydrometeorological and climatic pressures. Although droughts, floods, and shifting precipitation patterns are natural forcing mechanisms, their impacts are often intensified by anthropogenic interventions such as excessive water abstraction, land use changes, and hydraulic infrastructure modifications. The combination of climatic and human drivers poses a fundamental challenge for water resource managers. The understanding of the underlying forcing mechanisms of meteorological and hydrological droughts, hydrometeorological extremes and water scarcity, as well as their quantitative impact on water resources is essential. Especially under uncertain future climate conditions, the development of efficient water management plans and adaptation measures is imperative. Consequently, the success of any water management strategy under the WFD depends on the understanding of: (1) how meteorological droughts propagate into hydrological droughts, (2) how hydrometeorological extremes alter flow regimes, and (3) how these processes are impacted by localized human pressures.

Understanding these complications, the present study supports the notion that the PoMs within the RBMPs must evolve beyond their conventional focus. The traditional PoMs typically prioritize the mitigation of pollution, habitat degradation, and direct water-use conflicts, often overlooking climatic variability. However, achieving water resilience under the WFD, especially in a climate-vulnerable region like the Mediterranean, requires

effective PoMs that not only address traditional pressures but also integrate adaptation to meteorological and hydrological droughts, and climate-induced water scarcity. Consequently, the development of PoMs should be based not only on average conditions or historical extremes, but also on a range of plausible future scenarios that cover both climatic variation and abrupt hydrometeorological events. Additionally, the PoMs must be flexible enough to distinguish between short-term crisis responses and long-term structural adaptations. In this context, the integration of physically based models, climate projections, drought indices, and quantitative flow boundaries into the PoMs' design process is a key prerequisite for evidence-based water resource management. The framework for the design of PoMs under the WFD proposed in this study is centered on quantitative thresholds that trigger predefined adaptation actions and measures. Based on low-flow boundaries, drought indices, and modeled river responses under various climate scenarios, the framework defines clear thresholds that trigger warnings. Each warning level corresponds to a specific suite of actions, ranging from drought emergency plan development to mandatory abstraction restrictions, drought-resilient crop shifting, and NbS initiatives.

The operational feasibility of this framework was illustrated through its application to the Spercheios river basin, which was selected as a representative demonstration site. While the results are promising and suggest potential applicability in Greece and other regions, further testing across diverse hydrological, climatic, and socio-economic settings is required before broader transferability can be confirmed. In this case study, a process-based hydrological model was coupled with climate change projections to simulate future flow regimes under multiple emission scenarios. Additionally, drought indices and ecologically relevant low-flow boundaries were employed to quantify the impacts of climatic and anthropogenic pressures on the river's quantitative status. This approach enabled a clear differentiation between water scarcity driven by future climate uncertainty and water scarcity exacerbated by local human interventions. Based on the results of the water management plan adopted and evaluated for its effectiveness, the climatic variability poses a more significant pressure than the anthropogenic one. Furthermore, the findings of this study indicate that the adoption of a single action may not be sufficient; instead, a combination of actions is required for effective climate change mitigation. Ultimately, this application demonstrates that the proposed framework is not merely a theoretical construct but a practical, transferable guideline. It equips decision-makers and stakeholders with a concrete, evidence-based toolkit for designing adaptive PoMs that fulfill the WFD's objectives, enhance water resilience, and provide a structured toolbox for mitigating the hydrometeorological extremes and climate change pressures in Greece and beyond.

Author Contributions: Conceptualization, A.M., P.K., A.P. and E.D.; methodology, A.M. and E.D.; formal analysis, A.M.; investigation, A.M.; resources, E.D.; data curation, P.K., A.P. and E.D.; writing—original draft preparation, A.M.; writing—review and editing, P.K., A.P. and E.D.; visualization, A.M.; supervision, P.K., A.P. and E.D. All authors have read and agreed to the published version of the manuscript.

Funding: This research received no external funding.

Data Availability Statement: Data subject to third party restrictions. Data were obtained from the project "Monitoring of the ecological water quality of rivers, coastal and transitional waters of Greece to implement the Article 8 of Water Framework Directive 2000/60/EC" (MIS 375880, 375881, 375882, 375883, 375884, 375885) funded by the Operational Program "Environment and Sustainable Development" 2007–2013, financed by the European Regional Development Fund and the project "Monitoring and recording of the status (quality, quantity, pressures, and uses) of surface waters of Greece" (MIS 5001676) funded by the Operational Program "Transport infrastructure, environment and sustainable development" 2014–2020, financed by European Regional Development Fund. Aggregated data are available at http://nmwn.ypeka.gr/ (accessed on 1 May 2026), https:

//wfd24.hcmr.gr/ (accessed on 1 May 2026) and https://edp.ypen.gr/ (accessed on 1 May 2026). Disaggregated data were used with the permission of Ministry of Environment and Energy of Greece. Data from Region of Central Greece were available on request. Projected climate data of the CMIP6-GCM can be freely accessed in the Copernicus Climate Change Service (https://cds.climate.copernicus.eu/ (accessed on 1 May 2026)). The model setup and configuration files used in this study are available from the corresponding author upon reasonable request.

Acknowledgments: The hydrological simulations were conducted using the MIKE SHE 2025 and MIKE+ 2025 Student License.

Conflicts of Interest: The authors declare no conflicts of interest.

Abbreviations

The following abbreviations are used in this manuscript:

ACCESS-CM2	Australian Community Climate and Earth System Simulator Climate Model Version 2
AEMET	Agencia Estatal de Meteorología
AORI	Atmosphere and Ocean Research Institute, The University of Tokyo
AR	Assessment Reports
ARCCSS2	Australian Research Council Centre of Excellence for Climate System Science
BSC	Barcelona Supercomputing Center
C3S	Copernicus Climate Change Service
CEMS	Copernicus Emergency Management Service
CERFACS	Centre Européen de Recherche et de Formation Avancée en Calcul Scientifique
CI	Confidence Intervals
CICERO	Center for International Climate and Environmental Research
CMCC	Centro Euro-Mediterraneo sui Cambiamenti Climatici
CMCC-ESM2	Euro-Mediterranean Centre on Climate Change- Earth System Model version 2
CMIP6	sixth phase of the Coupled Model Intercomparison Project
CNR	Consiglio Nazionale delle Ricerche
CNRM	Centre National de Recherches Météorologiques
CNRM-ESM2-1	Centre National de Recherches Météorologiques- Earth system model-second generation
CSIRO	Commonwealth Scientific and Industrial Research Organisation
DHI	Danish Hydraulic Institute
DMI	Danish Meteorological Institute
dr	Refined Index of agreement
DWD	Drinking Water Directive 2020/2184
EC-Earth3-CC	Earth Consortium 3 Carbon Cycle
EDO	European Drought Observatories
ET	evapotranspiration
EU	European Union
FD	Floods Directive 2007/60/EC
FDR	false discovery rate
FMI	Finnish Meteorological Institute
GCM	General Circulation Models
GDO	Global Drought Observatory
GHG	greenhouse gases
HCMR	Hellenic Centre for Marine Research
IMBRIW	Institute of Marine Biological Resources and Inland Waters
INM	Institute for Numerical Mathematics Russian Federation
INM-CM5-0	Institute for Numerical Mathematics Climate Model version 5, experiment 0
IPCC	Intergovernmental Panel on Climate Change
JAMSTEC	Japan Agency for Marine-Earth Science and Technology

KGE	Kling–Gupta efficiency
KNMI	Koninklijk Nederlands Meteorologisch Instituut- Royal Netherlands Meteorological Institute
MAE	Mean Absolute Error
MET-Norway	Norwegian Meteorological Institute
MIROC6	Model for Interdisciplinary Research on Climate version 6
MK	Mann–Kendall
MME	multi-model ensemble method
MRI	Meteorological Research Institute of Japan
MRI-ESM2-0	Meteorological Research Institute Earth System Model version 2.0
MSE	Mean Square Error
NCCAS	National Climate Change Adaptation Strategy
ND	Nitrate Directive
NERSC	Nansen Environmental and Remote Sensing Center
NIES	National Institute for Environmental Studies
NILU	Norwegian Institute for Air Research
NorESM2-MM	Norwegian Earth System Model version 2—Medium Resolution (atmosphere and land)/Medium Resolution (ocean and sea-ice)
NSE	Nash-Sutcliffe coefficient
OL	Overland Flow
PBIAS	Percent bias
PoMs	Program of Measures
R	Pearson's correlation coefficient
R2	coefficient of determination
RAAPs	Regional Adaptation Action Plans
RBMPs	River Basin Management Plans
R-CCS	RIKEN Center for Computational Science
RMSE	Root Mean Square Error
RSR	RMSE to Standard Deviation Ratio
SMHI	Sveriges meteorologiska och hydrologiska institut—Swedish Meteorological and Hydrological Institute
SPEI	Standardized Precipitation Evapotranspiration Index
SPI	Standardized Precipitation Index
SSP	Socioeconomic Pathways
SZ	Saturated Zone
UiB	University of Bergen
UiO	University of Oslo
UZ	Unsaturated Zone
UNI	Uni Research
WFD	Water Framework Directive 2000/60
WGI	Working Group I
WHO	World Health Organization

Appendix A. Hydrological Model Setup

Hydrological models require a compromise between output accuracy and computational resources [149]. Considering these limitations and based on the data availability, the hydrological simulation of the Spercheios river basin was based on the following modules [61]:

- Overland Flow (OL): The subcatchment-based surface runoff method was chosen, which provides flexibility in terms of data requirements and model setup, and significantly reduces the computational time. This method is based on an empirical relation between flow depth and surface detention, and together with the Manning equation describes the discharge under turbulent flow conditions [150].

- Unsaturated Zone (UZ): The 2-Layer Water Balance Method used considers two "layers" representing average conditions at the unsaturated zone (the root zone and the zone between the roots and the water table) [151].
- Evapotranspiration (ET): The Two-Layer UZ/ET model was included to provide an estimate of the actual evapotranspiration and the amount of water that recharges the saturated zone. The specific approach divides the unsaturated zone into a root zone, from which ET processes may take place, and a zone below the root zone, where ET processes do not occur [151].
- Saturated Zone (SZ): The Linear Reservoir method [152] used is a combined lumped/physically distributed approach. It has been developed to provide a reliable solution for watershed water balance assessment, runoff simulation, flood prediction, and land use change impact on hydrological process assessment. The infiltrating water from the unsaturated zone may either contribute to the baseflow or move laterally as interflow towards the stream. Hence, the interflow reservoirs have two outlets, one outlet that contributes to the next interflow reservoir or the river, and the other that contributes to the baseflow reservoirs. Based on this method, the catchment area was subdivided into subcatchments, within which the saturated zone was represented by a series of interdependent, shallow interflow reservoirs, plus several deep groundwater reservoirs that contribute to stream baseflow separately [153].

The necessary inputs to the hydrological model were the following:

- The wider study area contains 11 high-quality meteorological stations monitoring daily precipitation. The data series of these stations have been imputed and homogeneity analysis has been performed under the 2nd Update of the River Basin Management Plans [154]. The location and altitude of the available stations represent quite well the topography and geographical coverage of the particular catchment. The density of the precipitation network is about 150 km^2/station and can be considered sufficient, based on the WHO recommendations regarding the minimum densities of recording precipitation stations [155]. The precipitation data were interpolated across a model domain using the Thiessen Polygon methodology [156]. The precipitation lapse rate of the study area was calculated to be 57 m/100 m (correlation coefficient R: 0.82, the *p*-value is 0.001997, and the result is significant at 5% confidence level—$p < 0.05$).
- The lack of the necessary climatological data (relative humidity, solar radiation and wind speed) precluded the use of the Penman–Monteith equation [107] for the estimation of daily reference evapotranspiration (ET). Therefore, ET was estimated using the temperature-based Hargreaves empirical approach [108], which is recommended only in cases of lack of other meteorological data and is considered to provide satisfactory results with an error rate of 10–15% or 1 mm/d, whichever is higher [109].
- In this study area, the land use–vegetation map was created after CORINE Land Cover CLC2018 data [157]. For each land use–vegetation class, time-varying values of LAI (Leaf Area Index), Root (Root depth) and Kc (crop coefficient) were attributed in the vegetation property file based on bibliography [158], and adjusted when necessary during the calibration procedure.
- The Irrigation Command Areas module of MIKE SHE was used to describe the water sources and irrigation techniques applied. Relevant information was retrieved from Local Organizations of Land Reclamation (LOLR). For the areas in which crops are irrigated through the public network, it was assumed that the irrigation was accomplished through the irrigation and drainage network. This network channeled water from rivers (if they are near them) or groundwater (for areas further away from irrigation channels).

- In order to calculate the water demand of the cultivation patterns of the Spercheios river basin, the spatial crop distribution from the Census of Agricultural and Livestock Holdings 1999–2000 [159] per municipal unit was used. These data were acquired after personal communication [65]. The estimation of the net irrigation requirement (*IR*) of the crops in the study area was based on the Food and Agriculture Organization (FAO) methodology [160]: $IR = ETc - (Pe + Ge + Wb)$, where *IR* = net irrigation requirement, *ETc* = crop evapotranspiration, *Pe* = effective dependable rainfall, *Ge* = groundwater contribution from the water table, and *Wb* = water stored in the soil at the beginning of each period (all in mm/month).
- In addition to the public boreholes used to meet irrigation and water supply needs of the area, numerous private boreholes operate in the Spercheios river basin. Based on the National Inventory of Water Abstraction Points [161], 774 active water abstraction sites (boreholes, wells, springs, etc.) have been registered in the study area. Based on the most recent update [135], the total water abstractions for the groundwater bodies of the Spercheios river basin were calculated to be about 94×10^6 m^3/y.
- In the present study, apart from the Spercheios river main branch, an additional eleven branches/tributaries were included. For each river branch, cross-sections and boundary and initial conditions were defined. Special care was taken during the river's downstream complex delineation (river diversion, Lamia ditch). Additionally, the most important engineering structures on the river network were included in the simulation (7 bridges and one weir-distributor). Data regarding the cross-sections' geometry were retrieved from the 2 × 2 m Digital Elevation Model (DEM) of the study area. This dataset has been produced from air photos taken between 2014 and 2016 [162]. Additionally, topographic field measurements conducted in 2014 in seven (7) cross-sections along the Spercheios main river branch were included [163]. Information regarding the geometric characteristics of the river structures were derived from the 1st Update of the Flood Risk Management Plan of the River Basin District of Eastern Central Greece [164].
- The spatial distribution of the soil characteristics of the Spercheios river basin were based on the corresponding hydrolithological map of the area, due to lack of a detailed soil map of the Spercheios river basin. Based on this approach, the characteristics of the weathered parent formations were defined (water content at saturation, water content at field capacity, water content at wilting point, and saturated hydraulic conductivity). The initial definition of the soil properties of each class was accomplished using bibliographical data [165–167], while they were also adjusted during the calibration procedure.
- Based on the linear reservoir method, the interflow reservoir approach used the route near surface groundwater of the unsaturated zone to local streams and rivers. The interflow reservoir discrimination was based on the topographic, geomorphological and hydrographic characteristics of the Spercheios river basin. The baseflow reservoir spatial distribution has been defined based on the hydrogeological characteristics of the study area [168].

Appendix B. Hydrological Model Calibration Criteria

The performance of the hydrological model of the Spercheios river basin was evaluated based on the following error metrics: goodness of fit, index of agreement and efficiency criteria: Mean Absolute Error—*MAE*, Mean Square Error—*MSE*, Root Mean Square Error—*RMSE*, Pearson's correlation coefficient—*R* [74], coefficient of determination—*R*2 [75], Nash–Sutcliffe coefficient—*NSE* [76], Percent bias—*PBIAS*, RMSE to Standard Deviation Ratio—*RSR*, Kling–Gupta efficiency—*KGE* [77,78], Refined Index of agreement—*dr* [79,80].

The goodness of fit scores R and $R2$ are widely used in hydrological modeling performance interpretation, with values closer to 1 indicating good model predictability. $R2$ values higher than 0.5 are generally considered acceptable in hydrological modelling [169]. Additionally, when $R2$ is used as efficient criteria, the gradient a and the intercept b of the regression should also be considered, with best fit to be accomplished when b is closer to 0 and a closer to 1 [79,170]. The main disadvantages of R and $R2$ scores are that they do not quantify bias and are sensitive to outliers [171,172].

The best fit for the error metrics *MAE*, *MSE*, *RMSE*, *RSR* and *PBIAs* is 0, while *RMSE* is the most sensitive to outliers [173]. Negative *PBIAS* values indicate overestimation, while positive values indicate underestimation [174].

The index of agreement *dr* ranges between -1 and 1, with 1 indicating the best model performance [80].

Model efficiency criteria *NSE* and *KGE* range between minus infinity and 1, with 1 being the optimal value. *NSE* is sensitive to extreme values and underestimates high peak flows [77]; values lower than 0 indicate that the mean observed value is a better predictor than the simulated value, and thus the model predictability is unsatisfactory, while values higher than zero are generally considered acceptable [175]. Additionally, when interpreting *NSE* values, the sample size must be taken into consideration [176]. *KGE* combines correlation coefficient, variability ratio and bias ratio statistical metrics into a single measure of model performance; the tendency of *KGE* underestimation is lower than the one reported in the *NSE* metric [77].

The criteria proposed by Moriasi et al. [177] concerning $R2$, *NSE* and *PBIAS* ($R2 \geq 0.60$, $NSE \geq 0.50$, $PBIAS \leq \pm 15\%$ for satisfactory performance) and by Knoben et al. [175] concerning *KGE* ($KGE > -0.41$) regarding hydrological model performance interpretation were employed.

Finally, visual tools, such as scatter plots, Bland–Altman plots [178] and cumulative frequency distribution (CDF) plots, were employed. The Bland–Altman plots specifically allow the user to quantify the agreement between two quantitative measurements using statistical limits (95% statistical limits of agreement—LoA, represented by ± 1.96 standard deviations of the mean). Additionally, these plots may provide information concerning systematic bias and outliers [179]. The 10% percentile of the cumulative frequency distribution of daily water level or discharge time-series was used as a low-flow indicator, while the 95% percentile of the cumulative frequency distribution of daily water level or discharge time-series was used as a high-flow indicator. The corresponding percentiles of river discharge are widely used as low- and high-flow indicators, respectively [180–182].

It should be noted that based on the central limit theorem, when the sample size of an independent random variable (daily discharge or water level) is sufficient, the normal distribution of the mean can be presumed, even if the original variables are not normally distributed [183]. The sample size required varies and depends on the skewness of the dataset. For highly skewed distributions or data containing outliers, a sample size over 70 or 100 is required for normal distribution to be assumed [184,185].

Appendix C. Hydrological Model Performance

In Table A1, the efficient criteria calculated for the calibration period for the monitoring stations of the Spercheios river basin are presented. Overall, there is a satisfactory agreement between the predicted and observed values of water level or discharge (Figures A1 and A2). During calibration, the correlation coefficient R ranged between 0.68 and 0.78 and can be characterized as high, except in the case of Komma station, which was calculated to be 0.48 and can be characterized as moderate [186]. The p-value was < 0.00001, and therefore the results were significant at $p < 0.01$. The coefficient of determination $R2$

was estimated to be between 0.46 and 0.60 and was acceptable [169], except for Gorgopotamos station, which was 0.25. The values of gradient a indicate an underestimation of the model's predictability, while the values of intercept b were close to zero in the cases of Asopos and Inachos stations, and high in the cases of Kastri and Gorgopotamos. The *MAE*, *MSE* and *RMSE* values were small and close to zero, except for the cases of Kompotades and Inachos stations. *RSR* values were higher than the optimum 0.70 value for satisfactory performance [169], except for Asopos station, where the *RSR* was 0.68, while in the case of Gorgopotamos, the *RSR* value was higher than 0.80. *PBIAS* was close to 0% in all cases, except for Inachos station. The error metrics *MAE*, *RMSE* and *PBIAS* were positive, supporting the conclusion that the predicted values were underestimated. The index of agreement *dr* was positive in all cases and ranged between 0.60 and 0.67, indicating the satisfactory performance of the model.

NSE values were higher than zero in all stations examined, indicating acceptable performance of the model. At Kompotades and Komma stations, *NSE* was near 0.50, and at Asopos, it was higher than 0.50, indicating satisfactory performance. *KGE* ranged between 0.62 and 0.76, except for Gorgopotamos and Komma stations, where it was calculated to be 0.24 and 0.43, respectively. It should be highlighted that the sample size at monitoring stations Kastri, Kompotades, Gorgopotamos and Komma was extremely high. Finally, *KGE* values were in all cases positive and higher than 0.30 (except for the case of Gorgopotamos station, where it was 0.24), indicating that the model is behavioral, and therefore the model performance acceptable.

Based on the criteria proposed by Moriasi [177], the model can be characterized as satisfactory regarding the coefficient of determination $R2$ at monitoring stations Asopos and Inachos ($R2 \geq 0.60$), at Asopos station regarding *NSE* ($NSE \geq 0.50$), and at all stations except Inachos regarding *PBIAS* ($PBIAS \leq \pm 15\%$). Regarding the *KGE* criterion [175], the model performance was satisfactory at all stations examined ($KGE > -0.41$).

Based on the Bland–Altman plots, most of the values were between the 95% statistical limits of agreement—LoA (represented by ± 1.96 standard deviations of the mean). Therefore, it can be assumed that there was an acceptable agreement between observed and predicted discharge values at all monitoring stations examined. The underestimation of some measurements was confirmed, while outliers can also be reported, especially in the cases of Kastri, Kompotades, Gorgopotamos and Komma stations. The LoA values at all stations were quite small, indicating good agreement, although the scatter around the bias line grows larger as the average of the measurements grows higher and positive, indicating that the model did not always predict high flows of the river successfully (Figures A1iii,vi,ix and A2iii,vi,ix).

In Figure A3, the cumulative frequency distribution plots of daily observed and predicted water level time-series are presented (calibration procedure). These plots support the conclusion of the acceptable performance of the hydrological model. Based on the results, the model did not manage to accurately predict low flows at Gorgopotamos and Komma stations or high flows at Komma station. On the contrary, the model successfully predicted both low and high flows at Kastri station (Table A2).

Based on the results of the validation procedure, the hydrological model performance can be confirmed (Table A1, Figure A4). The correlation coefficient R can be characterized as high (>0.70) in all cases except for Alamana station, which can be characterized as moderate (0.53) [186]. The p-value was <0.00001 in all cases, and therefore the results were significant at $p < 0.01$. The coefficient of determination $R2$ ranged between 0.52 and 0.56 and was acceptable [177], except for Alamana station (0.28). The values of gradient a also indicated the model underestimation, while the values of intercept b were close to zero at Anthili and Makri stations. The *MAE*, *MSE* and *RMSE* values were small and close to zero, except for

the case of Makri station. *RSR* values were close to or higher than the optimum 0.70 value for satisfactory performance [169], while in the case of Alamana, it was higher than 0.80. *PBIAS* was close to 0% in all cases except Makri station (11.6%). The error metrics *MAE*, *RMSE* and *PBIAS* were positive, supporting the conclusion that the predicted values were underestimated. The index of agreement *dr* was positive in all cases and ranged between 0.59 and 0.74, validating the satisfactory performance of the model.

Table A1. Efficiency criteria for the calibration and validation of the hydrological model of the Spercheios river basin. The metrics that meet the criteria regarding the model performance are noted in grey.

Calibration	***N***	***MAE***	***MSE***	***RMSE***	***R***	***R2***	***a***	***b***	***NSE***	***PBIAS***	***RSR***	***KGE***	***dr***	***p*-Value**
Kastri	11,139	0.18	0.06	0.25	0.69	0.47	27.01	0.66	0.39	0.0%	0.78	0.69	0.63	<0.00001 *
Kompotades	10,700	0.33	0.23	0.48	0.68	0.46	9.34	0.57	0.44	0.0%	0.75	0.64	0.64	<0.00001 *
Gorgopotamos	11,039	0.12	0.04	0.19	0.50	0.25	41.90	0.21	0.24	0.0%	0.87	0.24	0.60	<0.00001 *
Komma	10,010	0.19	0.07	0.27	0.69	0.48	6.29	0.36	0.45	0.0%	0.74	0.43	0.66	<0.00001 *
Asopos	40	0.07	0.01	0.10	0.76	0.58	0.04	0.74	0.53	1.1%	0.68	0.76	0.65	<0.00001 *
Inachos	41	0.37	0.25	0.50	0.78	0.60	0.30	0.62	0.51	16.0%	0.70	0.66	0.64	<0.00001 *
Validation	***N***	***MAE***	***MSE***	***RMSE***	***R***	***R2***	***a***	***b***	***NSE***	***PBIAS***	***RSR***	***KGE***	***dr***	***p*-value**
Alamana	1642	0.18	0.06	0.25	0.53	0.28	3.87	0.23	0.27	0.5%	0.86	0.26	0.59	<0.00001 *
Anthili	2388	0.11	0.02	0.15	0.72	0.52	1.23	0.64	0.49	0.0%	0.71	0.70	0.65	<0.00001 *
Makri	70	1.02	3.55	1.88	0.75	0.56	0.86	0.51	0.54	11.6%	0.68	0.58	0.74	<0.00001 *
T_Sper	63	0.31	0.16	0.40	0.73	0.53	6.50	0.58	0.53	0.0%	0.69	0.66	0.68	<0.00001 *

* The result is significant at $p < 0.01$. *N*: sample size. *ME*: Mean Error. *MAE*: Mean Absolute Error. *MSE*: Mean Squared Error. *RMSE*: Root Mean Square Error. *R*: Pearson's correlation coefficient. *a*: gradient. *b*: intercept. *R2*: Coefficient of determination. *NSE*: Nash–Sutcliffe coefficient. *PBIAS*: Percent bias. *RSR*: RMSE to Standard Deviation Ratio. *KGE*: Kling–Gupta Efficiency. *dr*: refined index of agreement.

NSE values were higher than zero at all stations examined during validation, indicating acceptable performance of the model, and higher than 0.50, except in the case of Alamana station (0.27). In the case of Alamana and Anthili stations, the sample size was very high. Finally, *KGE* values were in all cases positive, validating the acceptable performance of the model.

Based on the criteria proposed by Moriasi [177], the model cannot be characterized as satisfactory regarding the coefficient of determination *R*2 ($R2 \geq 0.60$), but was satisfactory for all stations except Alamana regarding *NSE* ($NSE \geq 0.50$) and at all stations regarding *PBIAS* ($PBIAS \leq \pm 15\%$). Regarding the *KGE* criterion [175], the model performance was satisfactory at all stations examined ($KGE > -0.41$), while only at Alamana station was *KGE* lower than 0.30 (0.26).

Based on the Bland–Altman plots, most of the values were between the 95% statistical limits of agreement—LoA (represented by ± 1.96 standard deviations of the mean). Therefore, it can be assumed that there was an acceptable agreement between observed and predicted discharge values at all monitoring stations examined. The underestimation of some measurements was confirmed, while outliers can also be reported, especially in the case of Alamana and Anthili stations. The LoA values at all stations were quite small, indicating good agreement, although the scatter around the bias line gets larger as the average of the measurements gets higher and positive, indicating that the model did not always predict high flows of the river successfully (Figure A4iii,vi,ix,xii).

In Figure A5, the cumulative frequency distribution plots of daily observed and predicted water level time-series are presented (validation procedure). These plots support the conclusion of the acceptable performance of the hydrological model. Based on the results, the model did not manage to accurately predict high flows at Alamana stations. On

the contrary, the model successfully predicted both low and high flows at Anthili station and low flows at Alamana station (Table A3).

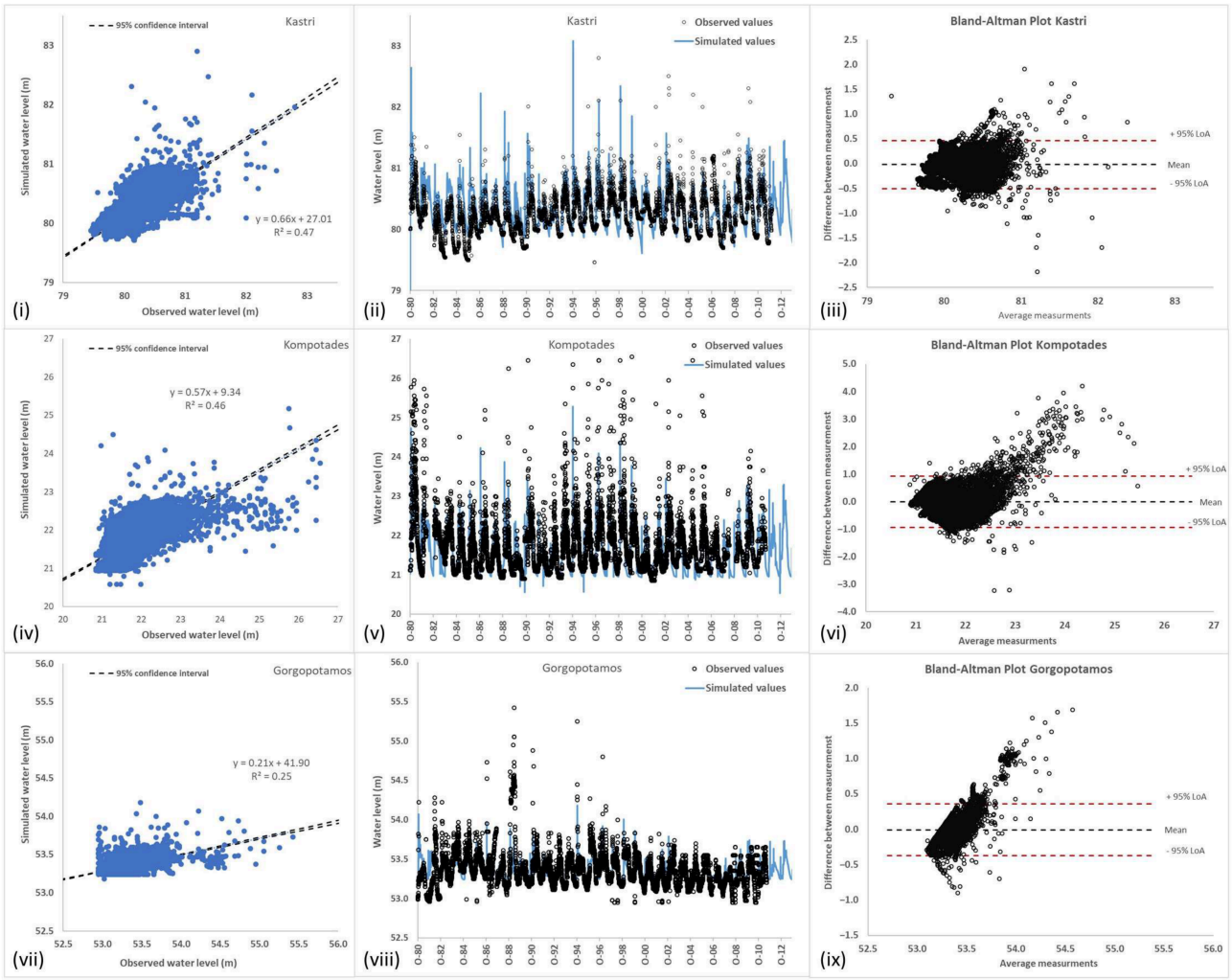

Figure A1. Simulated and observed discharge, and Bland–Altman plots for monitoring stations (**i–iii**) Kastri, (**iv–vi**) Kompotades, and (**vii–ix**) Gorgopotamos (calibration procedure).

Table A2. The 10%, 50% and 95% percentiles of observed and predicted daily water level time-series for Kastri, Kompotades, Gorgopotamos, and Komma stations.

Station		10%	50%	95%
Kastri	Observed (m)	79.86	80.19	80.75
	Predicted (m)	79.88	80.20	80.75
	Difference (m)	−0.02	−0.01	0.00
Kompotades	Observed (m)	21.05	21.45	22.70
	Predicted (m)	20.97	21.55	22.49
	Difference (m)	0.08	−0.10	0.21
Gorgopotamos	Observed (m)	53.14	53.33	53.69
	Predicted (m)	53.25	53.35	53.51
	Difference (m)	−0.11	−0.02	0.18
Komma	Observed (m)	9.39	9.71	10.46
	Predicted (m)	9.56	9.74	10.08
	Difference (m)	−0.17	−0.03	0.38

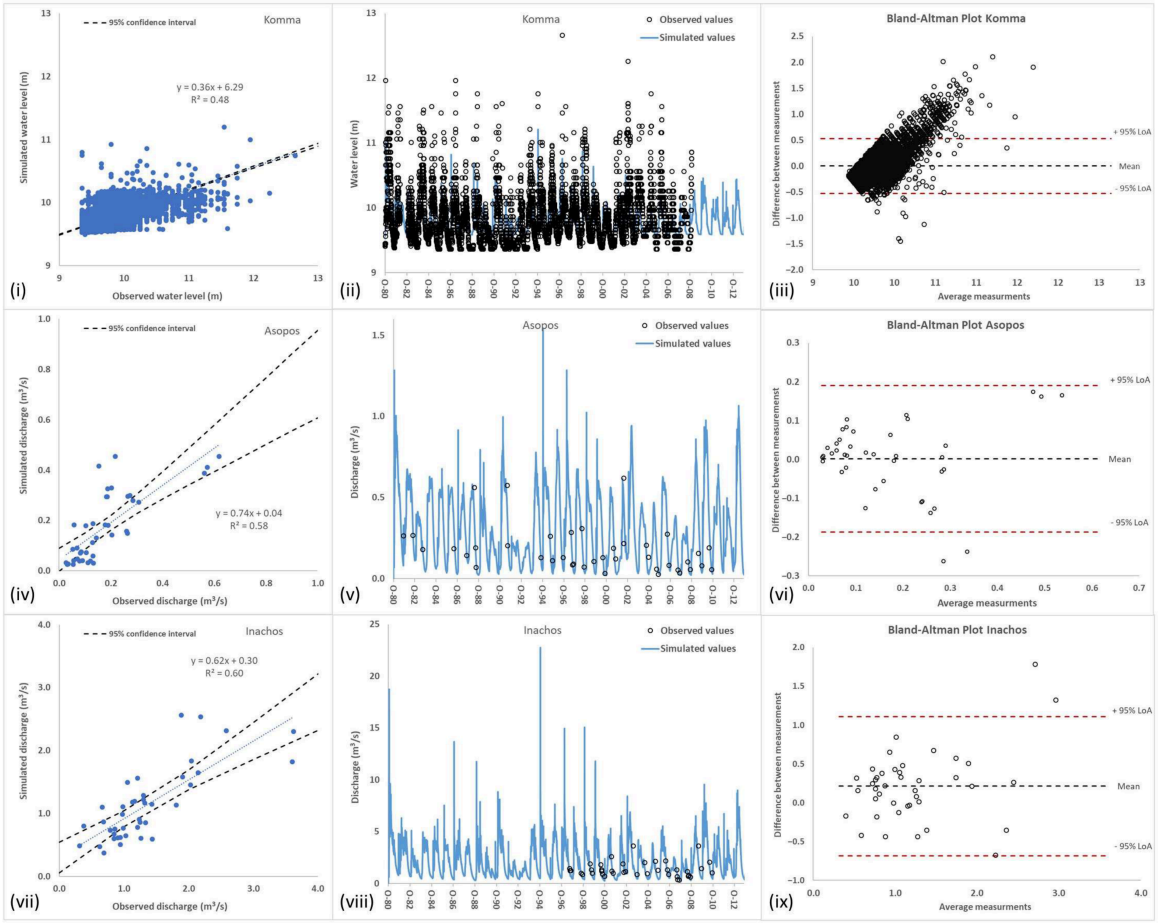

Figure A2. Simulated and observed discharge, and Bland–Altman plots for monitoring stations (**i–iii**) Komma, (**iv–vi**) Asopos, and (**vii–ix**) Inachos (calibration procedure).

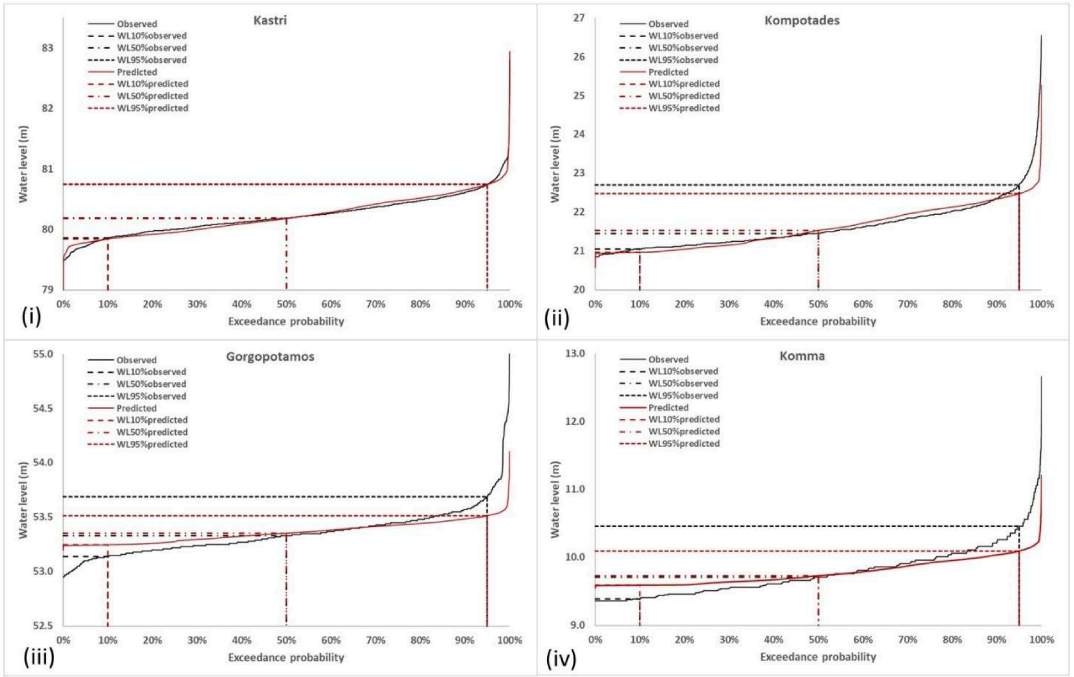

Figure A3. Cumulative frequency distribution plots of daily observed and predicted water level time-series for (**i**) Kastri, (**ii**) Kompotades, (**iii**) Gorgopotamos, and (**iv**) Komma stations.

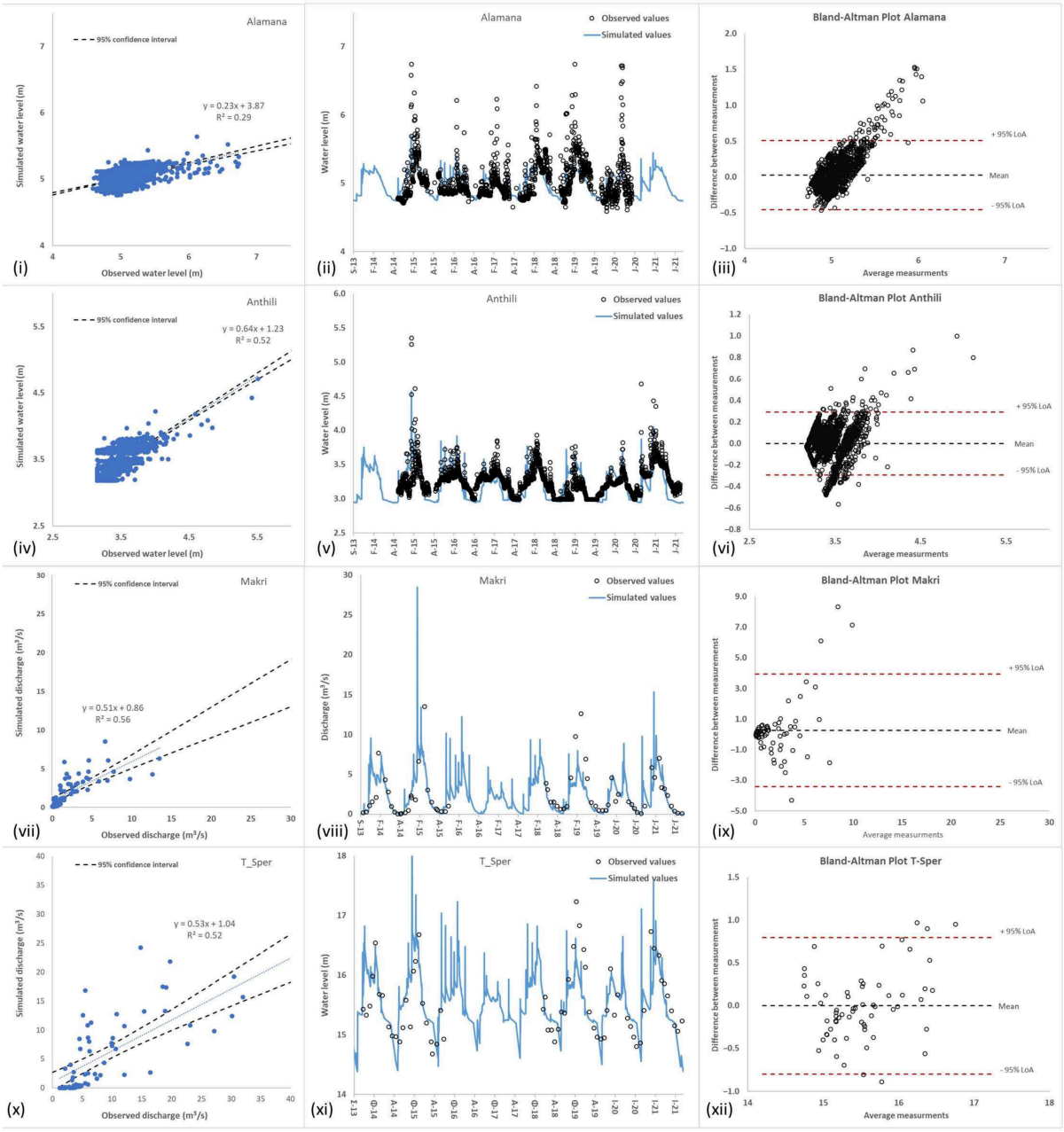

Figure A4. Simulated and observed discharge, and Bland–Altman plots for monitoring stations (**i–iii**) Alamana, (**iv–vi**) Anthili, (**vii–ix**) Makri, and (**x–xii**) T-Sper (validation procedure).

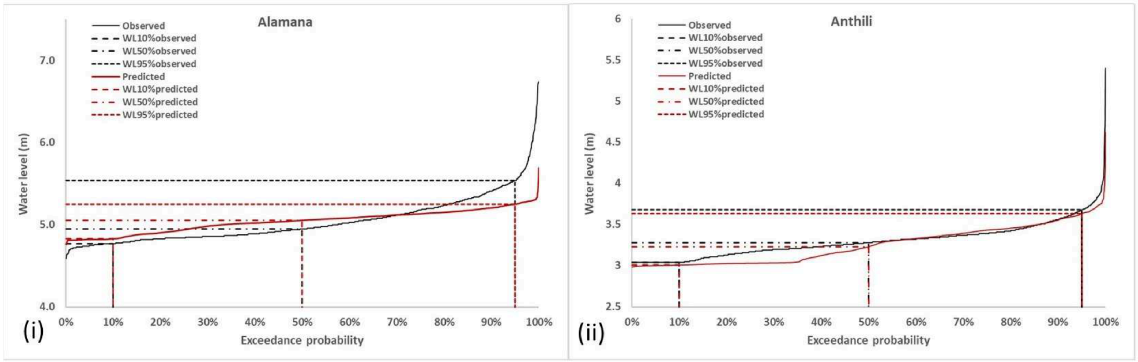

Figure A5. Cumulative frequency distribution plots of daily observed and predicted water level time-series for (**i**) Alamana and (**ii**) Anthili stations.



Figure A6. Examples of Spercheios river riverbed changes between the years 2007/09 and 2015/16: distributor construction near Komma (**i**), and riverbed alteration near (**ii**) Zilefto and (**iii**) Agios Georgios Tymfristou villages [187,188].

Table A3. The 10%, 50% and 95% percentiles of observed and predicted daily water level time-series for Alamana and Anthili stations.

Station		10%	50%	95%
Alamana	Observed (m)	4.77	4.95	5.54
	Predicted (m)	4.82	5.03	5.21
	Difference (m)	−0.05	−0.08	0.33
Anthili	Observed (m)	3.15	3.39	3.79
	Predicted (m)	3.19	3.40	3.70
	Difference (m)	−0.04	−0.01	0.09

Additionally, the subsurface groundwater exchange to adjacent basins, especially through the karstic formations that structure the northeastern and southern mountainous part of the study area, can be assumed [189,190]. This is a two-way dynamic and complicated hydrological process that is difficult to incorporate into the model, due to the lack of necessary spatio-temporal information. For this reason, it was not taken into consideration during the simulation.

Taking into consideration the above-mentioned limitations, the performance of the developed hydrological model can be considered acceptable for the purposes of the present study.

References

1. Bukaveckas, P.A. Rivers. In *Encyclopedia of Inland Waters*; Likens, G.E., Ed.; Academic Press: Cambridge, MA, USA, 2009; pp. 721–732.
2. Likens, G.E. *River Ecosystem Ecology: A Global Perspective. A Derivative of Encyclopedia of Inland Waters*; Academic Press: Cambridge, MA, USA, 2010.
3. Palmer, M.; Ruhi, A. Linkages between Flow Regime, Biota, and Ecosystem Processes: Implications for River Restoration. *Science* **2019**, *365*, eaaw2087. [CrossRef]
4. Ward, J.V. The Four-Dimensional Nature of Lotic Ecosystems. *J. N. Am. Benthol. Soc.* **1989**, *8*, 2–8. [CrossRef]
5. Poff, N.L.; Allan, J.D.; Bain, M.B.; Karr, J.R.; Prestegaard, K.L.; Richter, B.; Sparks, R.E.; Stromberg, J.C. The Natural Flow Regime. *Bioscience* **1997**, *47*, 769–784. [CrossRef]
6. Zeiringer, B.; Seliger, C.; Greimel, F.; Schmutz, S. River Hydrology, Flow Alteration, and Environmental Flow. In *Riverine Ecosystem Management. Aquatic Ecology Series 8*; Schmutz, S., Sendzimir, J., Eds.; Springer: Cham, Switzerland, 2018; pp. 67–89.
7. Pickett, S.T.A.; White, P.S. *The Ecology of Natural Disturbance and Patch Dynamics*; Academic Press: Orlando, FL, USA, 1985.
8. Bunn, S.; Arthington, A. Basic Principles and Ecological Consequences of Altered Flow Regimes for Aquatic Biodiversity. *Environ. Manag.* **2002**, *30*, 492–507. [CrossRef] [PubMed]
9. Collier, C.G. *Hydrometeorology*; John Wiley & Sons, Ltd.: Chichester, UK, 2016.
10. Valipour, M.; Bateni, S.; Dalezios, N.; Almazroui, M.; Heggy, E.; Şen, Z.; Angelakis, A.N. Hydrometeorology: Review of Past, Present and Future Observation Methods. In *Hydrology*; Hromadka, T., Rao, P., Eds.; IntechOpen: London, UK, 2020; pp. 1–28.
11. Moiseenko, T. Surface Water under Growing Anthropogenic Loads: From Global Perspectives to Regional Implications. *Water* **2022**, *14*, 3730. [CrossRef]
12. Ray, R.; Getachew Tikuye, B. Impact of Climate Change on Surface Water Resources. In *Limnology—Surface and Groundwater Ecosystems*; Ray, R., Tikuye, G., Summers, B., Eds.; IntechOpen: London, UK, 2025; Volume 32, pp. 1–14.
13. Free, G.; Poikane, S.; Solheim, A.; Bussettini, M.; Bradley, C.; Smith, J.; Caroni, R.; Bresciani, M.; Pinardi, M.; Giardino, C.; et al. Climate Change and Ecological Assessment in Europe under the WFD—Hitting Moving Targets with Shifting Baselines? *J. Environ. Manag.* **2024**, *370*, 122884. [CrossRef]
14. Döll, P.; Zhang, J. Impact of Climate Change on Freshwater Ecosystems: A Global-Scale Analysis of Ecologically Relevant River Flow Alterations. *Hydrol. Earth Syst. Sci.* **2010**, *14*, 783–799. [CrossRef]
15. Caretta, M.A.; Mukherji, A.; Arfanuzzaman, M.; Betts, R.A.; Gelfan, A.; Hirabayashi, Y.; Lissner, T.K.; Liu, J.; Lopez Gunn, E.; Morgan, R.; et al. Water. In *Climate Change 2022: Impacts, Adaptation and Vulnerability. Contribution of Working Group II to the Sixth Assessment Report of the Intergovernmental Panel on Climate Change*; Cambridge University Press: Cambridge, UK; New York, NY, USA, 2022; pp. 551–712.
16. Ali, E.; Cramer, W.; Carnicer, J.; Georgopoulou, E.; Hilmi, N.; Le Cozannet, G.; Lionello, P. Cross-Chapter Paper 4: Mediterranean Region. In *Climate Change 2022: Impacts, Adaptation and Vulnerability. Contribution of Working Group II to the Sixth Assessment Report of the Intergovernmental Panel on Climate Change*; Pörtner, H., Roberts, D., Tignor, M., Poloczanska, E., Mintenbeck, K., Alegría, A., Craig, M., Langsdorf, S., Löschke, S., Möller, V., et al., Eds.; Cambridge University Press: Cambridge, UK; New York, NY, USA, 2022; pp. 2233–2272.
17. Douville, H.; Raghavan, K.; Renwick, J.; Allan, R.P.; Arias, P.A.; Barlow, M.; Cerezo-Mota, R.; Cherchi, A.; Gan, T.Y.; Gergis, J.; et al. Water Cycle Changes. In *Climate Change 2021: The Physical Science Basis. Contribution of Working Group I to the Sixth Assessment Report of the Intergovernmental Panel on Climate Change*; Masson-Delmotte, V., Zhai, P., Pirani, A., Connors, S.L., Péan, C., Berger, S., Caud, N., Chen, Y., Goldfarb, L., Gomis, M.I., et al., Eds.; Cambridge University Press: Cambridge, UK; New York, NY, USA, 2021; pp. 1055–1210.
18. Gudmundsson, L.; Boulange, J.; Do, H.; Gosling, S.; Grillakis, M.; Koutroulis, A.; Leonard, M.; Liu, J.; Schmied, H.; Papadimitriou, L.; et al. Globally Observed Trends in Mean and Extreme River Flow Attributed to Climate Change. *Science* **2021**, *371*, 1159–1162. [CrossRef]

19. Seneviratne, S.; Zhang, X.; Adnan, M.; Badi, W.; Dereczynski, C.; Di Luca, A.; Ghosh, S.; Iskandar, I.; Kossin, J.; Lewis, S.; et al. Weather and Climate Extreme Events in a Changing Climate. In *Climate Change 2021: The Physical Science Basis. Contribution of Working Group I to the Sixth Assessment Report of the Intergovernmental Panel on Climate Change*; Masson-Delmotte, V., Zhai, P., Pirani, A., Connors, S., Péan, C., Berger, S., Caud, N., Chen, Y., Goldfarb, L., Gomis, M., et al., Eds.; Cambridge University Press: Cambridge, UK; New York, NY, USA, 2021; pp. 1513–1766.
20. Wu, G.; Chen, J.; Shi, X.; Kim, J.; Xia, J.; Zhang, L. Impacts of Global Climate Warming on Meteorological and Hydrological Droughts and Their Propagations. *Earths Future* **2022**, *10*, e2021EF002542. [CrossRef]
21. Tramblay, Y.; Koutroulis, A.; Samaniego, L.; Vicente-Serrano, S.; Volaire, F.; Boone, A.; Le Page, M.; Llasat, M.; Albergel, C.; Burak, S.; et al. Challenges for Drought Assessment in the Mediterranean Region under Future Climate Scenarios. *Earth. Sci. Rev.* **2020**, *210*, 103348. [CrossRef]
22. Parmesan, C.; Morecroft, M.D.; Trisurat, Y.; Adrian, R.; Anshari, G.Z.; Arneth, A.; Gao, Q.; Gonzalez, P.; Harris, R.; Price, J.; et al. Terrestrial and Freshwater Ecosystems and Their Services. Contribution of Working Group II to the Sixth Assessment Report of the Intergovernmental Panel on Climate Change. In *Climate Change 2022—Impacts, Adaptation and Vulnerability*; Cambridge University Press: Cambridge, UK; New York, NY, USA, 2023; pp. 197–377.
23. Rolls, R.; Leigh, C.; Sheldon, F. Mechanistic Effects of Low-Flow Hydrology on Riverine Ecosystems: Ecological Principles and Consequences of Alteration. *Freshw. Sci.* **2012**, *31*, 1163–1186. [CrossRef]
24. Bradford, M.; Heinonen, J. Low Flows, Instream Flow Needs and Fish Ecology in Small Streams. *Can. Water Resour. J.* **2008**, *33*, 165–180. [CrossRef]
25. Rack, L.E.; Freeman, M.C.; Emanuel, B.N.; Craig, L.S.; Golladay, S.W.; Yang, C.; Wenger, S.J. How Low Is Too Low? Partnering with Stakeholders and Managers to Define Ecologically Based Low-Flow Thresholds in a Perennial Temperate River. *River Res. Appl.* **2024**, *40*, 1393–1416. [CrossRef]
26. Nilsson, C.; Renöfält, B. Synthesis, Part of a Special Feature on New Methods for Adaptive Water Management Linking Flow Regime and Water Quality in Rivers: A Challenge to Adaptive Catchment Management. *Ecol. Soc.* **2008**, *13*, 18.
27. Royer, T. Human-Dominated Rivers and River Management in the Anthropocene. In *Stream Ecosystems in a Changing Environment*; Jeremy, J., Stanley, E., Eds.; Academic Press: London, UK; Elsevier: London, UK, 2016; pp. 491–524.
28. Reid, A.; Carlson, A.; Creed, I.; Eliason, E.; Gell, P.; Johnson, P.; Kidd, K.; MacCormack, T.; Olden, J.; Ormerod, S.; et al. Emerging Threats and Persistent Conservation Challenges for Freshwater Biodiversity. *Biol. Rev.* **2019**, *94*, 849–873. [CrossRef]
29. European Parliament. Council of the European Union European Commission Council Directive 2000/60/EC of the European Parliament and of the Council of 23 October 2000 Establishing a Framework for Community Action in the Field of Water Policy. *Off. J. Eur. Communities* **2000**, *L327*, 1–72.
30. Council of the European Communities. Council Directive of 12 December 1991 Concerning the Protection of Waters against Pollution Caused by Nitrates from Agricultural Sources. *Off. J. Eur. Communities* **1991**, *L 375*, 1–8.
31. European Parliament. Council of the European Communities Directive 2007/60/EC of the European Parliament and of the Council of 23 October 2007 on the Assessment and Management of Flood Risks. *Off. J. Eur. Union* **2007**, *L 288*, 27–34.
32. European Parliament. Council of the European Union Directive (EU) 2020/2184 of the European Parliament and of the Council of 16 December 2020 on the Quality of Water Intended for Human Consumption (Recast). *Off. J. Eur. Union* **2020**, *L435*, 1–62.
33. European Commission. *River Basin Management in a Changing Climate—Common Implementation Strategy for the Water Framework Directive and the Floods Directive—Guidance Document No. 24*; Publications Office of the European Union: Luxembourg, 2024.
34. Dahal, D.; Bhattarai, N.; Silwal, A.; Shrestha, S.; Shrestha, B.; Poudel, B.; Kalra, A. A Review on Climate Change Impacts on Freshwater Systems and Ecosystem Resilience. *Water* **2025**, *17*, 3052. [CrossRef]
35. Ciampittiello, M.; Marchetto, A.; Boggero, A. Water Resources Management under Climate Change: A Review. *Sustainability* **2024**, *16*, 3590. [CrossRef]
36. European Commission. *Communication from the Commission to the European Parliament, the Council, the European Economic and Social Committee and the Committee of the Regions. European Water Resilience Strategy. COM/2025/280 Final*; European Commission, Directorate-General for Environment: Brussels, Belgium, 2025.
37. European Commission. *Communication from the Commission to the European Parliament, the Council, the European Economic and Social Committee and the Committee of the Regions. Forging a Climate-Resilient Europe—The New EU Strategy on Adaptation to Climate Change. COM/2021/82 Final*; European Commission, Directorate-General for Climate Action: Brussels, Belgium, 2021.
38. Charchousi, D.; Stathopoulou, E.; Kolitsi, G.; Leka, A.; Papadopoulou, M. Assessment of Regional Adaptation Strategies in Greece. *Atmosphere* **2026**, *17*, 288. [CrossRef]
39. Price, J. Assessing the Impact of Climate Change on Water Resources and Hydrological Cycles. *J. Biodivers. Bioprospecting Dev.* **2024**, *10*, 1. [CrossRef]
40. Soares, L.; Thouillot, M.; Frossard, V.; Desgué-Itier, O.; Barouillet, C.; Baulaz, Y.; Clément, J.C.; Domaizon, I.; Dorioz, J.M.; Goulon, C.; et al. Expanding the European Water Framework Directive Indicators to Address Long-Term Climate Change Impacts on Lakes Using Mechanistic Lake Models. *Ecol. Indic.* **2025**, *172*, 113220. [CrossRef]

41. European Commission. *Study on Adaptation Modelling. Comprehensive Desk Review: Climate Adaptation Models and Tools*; Directorate-General for Climate Action, CMCC, IVM and PWA: Brussels, Belgium, 2020.
42. Ministry of Environment and Energy of Greece. *National Strategy for Adaptation to Climate Change of Greece*; Ministry of Environment and Energy: Athens, Greece, 2016.
43. Assimacopoulos, D.; Sebos, I.; Chioti, D.; Katsiardi, P. Advancing Climate Change Adaptation in Greece: Development and Implementation of a National Monitoring and Evaluation System. *EuroMediterr. J. Environ. Integr.* **2025**, *10*, 4079–4090. [CrossRef]
44. Hellenic Republic. *National Energy and Climate Plan of Greece-Revised Edition*; Ministry of Environment and Energy: Athens, Greece, 2024.
45. Mentzafou, A.; Dimitriou, E.; Papadopoulos, A.; Katsafados, P. Low Flow Season River Discharge Boundaries Definition of Greek Rivers to Assess the Impact of Hydrometeorological and Climatic Pressures. *Hydrol. Sci. J.* 2026, *in press*. [CrossRef]
46. Hellenic Republic. FEK 5384/B/2021. Update of the Water Quality and Quantity National Monitoring Network, by Determining the Sites of Measurements and the Operating Agencies, in Alignment to the Article 4, Paragraph 4 of Law 3199/2003 (A'280). To Replace the Joint Ministerial Decision No. 140384/2011 (B'2017). *Gov. Gaz. Issue* **2021**, *B*, 69305–69340. (In Greek)
47. Psomiadis, E. Research of Geomorphological and Environmental Changes in the Sperchios' River Basin Utilizing New Technologies. Ph.D. Thesis, Agricultural University of Athens, Athens, Greece, 2010. (In Greek)
48. Navarro, D.; Lizundia-Loiola, J.; Paz, J.; Abajo, B.; Cantergiani, C.; García, G.; Feliu, E. *Updating and Integrating CLIMATE Datasets and Maps. Final Report EPSON 2020*; European Regional Development Fund: Luxembourg, 2022.
49. Mentzafou, A.; Varlas, G.; Dimitriou, E.; Papadopoulos, A.; Pytharoulis, I.; Katsafados, P. Modeling the Effects of Anthropogenic Land Cover Changes to the Main Hydrometeorological Factors in a Regional Watershed, Central Greece. *Climate* **2019**, *7*, 129. [CrossRef]
50. Mentzafou, A.; Markogianni, V.; Dimitriou, E. *Development of an Integrated Management System for Basin, Coastal and Marine Zones. Technical Report on the Spatiotemporal Changes of Environmental Parameters*; Hellenic Centre for Marine Research-Institute of Marine Biological Resources and Inland Waters: Anavyssos, Greece, 2015. (In Greek)
51. Mentzafou, A.; Wagner, S.; Dimitriou, E. Historical Trends and the Long-Term Changes of the Hydrological Cycle Components in a Mediterranean River Basin. *Sci. Total Environ.* **2018**, *636*, 558–568. [CrossRef]
52. Mentzafou, A.; Markogianni, V.; Papadopoulos, A.; Pavlidou, A.; Tziavos, C.; Dimitriou, E. The Impacts of Anthropogenic and Climatic Factors on the Interaction of Spercheios River and Maliakos Gulf, the Aegean Sea. In *The Aegean Sea Environment: Anthropogenic Presence and Impact*; Anagnostou, C., Kostianoy, A., Mariolakos, I., Panayotidis, P., Soilemezidou, M., Tsaltas, G., Eds.; Springer: Berlin/Heidelberg, Germany, 2020; pp. 1–33.
53. Kraft, J.C.; Rapp, G.; Szemler, G.J.; Tziavos, C.; Kase, E.W. The Pass at Thermopylae, Greece. *J. Field Archaeol.* **1987**, *14*, 181–198. [CrossRef]
54. Michail, M.; Chatzipetros, A. Morphotectonic Analysis of Faults in Sperchios Basin (Fthiotis, Central Greece). *Bull. Geol. Soc. Greece* **2013**, *47*, 295–304. [CrossRef]
55. Kilias, A.; Tranos, M.; Papadimitriou, E.; Karakostas, V. The Recent Crustal Deformation of the Hellenic Orogen in Central Greece; the Kremasta and Sperchios Fault Systems and Their Relationship with the Adjacent Large Structural Features. *Z. Der Dtsch. Ges. Geowiss.* **2008**, *159*, 533–547. [CrossRef]
56. Metaxas, A.; Varvarousis, G.; Karydakis, G.; Dotsika, E.; Papanikolaou, G. Geothermal Status of Thermopylae-Anthili Area in Fthiotida Prefecture. *Bull. Geol. Soc. Greece* **2010**, *2265*, 43–45.
57. Hellenic Republic Characterization and Inclusion in Category Geothermal Fields FEK 1058/B/2009. *Gov. Gaz. Issue* **2009**, *B*, 13489–13500. (In Greek)
58. Pechlivanidou, S. Modeling the Sedimentological and the Geomorphological Evolution of the Sperchios Deltaic Sequence During Holocene. Ph.D. Thesis, Aristotle University of Thessaloniki, Thessaloniki, Greece, 2012. (In Greek)
59. Karli, A. Hydrogeological & Hydrochemical Conditions of the Aquifers of Spercheios River Basin. Master's Thesis, University of Patra, Patra, Greece, 2013. (In Greek)
60. Tziavos, C. Sedimentology, Ecology, and Paleogeography of the Sperchios Valley and Maliakos Gulf, Greece. Master's Thesis, University of Delaware, Newark, DE, USA, 1977.
61. DHI. *MIKE SHE User Guide and Reference Manual*; Danish Hydraulic Institute: Hørsholm, Denmark, 2025.
62. Refsgaard, J.; Storm, B. Construction, Calibration and Validation of Hydrological Models. In *Distributed Hydrological Modelling*; Abbott, M.B., Refsgaard, J.C., Eds.; Springer: Dordrecht, The Netherlands, 1996; pp. 41–54.
63. Ma, L.; He, C.; Bian, H.; Sheng, L. MIKE SHE Modeling of Ecohydrological Processes: Merits, Applications, and Challenges. *Ecol. Eng.* **2016**, *96*, 137–149. [CrossRef]
64. DHI. *MIKE+ River Network Modelling User Guide*; Danish Hydraulic Institute: Hørsholm, Denmark, 2025.
65. Mentzafou, A.; Vamvakaki, C.; Zacharias, I.; Gianni, A.; Dimitriou, E. Climate Change Impacts on a Mediterranean River and the Associated Interactions with the Adjacent Coastal Area. *Environ. Earth Sci.* **2017**, *76*, 259. [CrossRef]

66. Paparrizos, S.; Maris, F. Hydrological Simulation of Sperchios River Basin in Central Greece Using the MIKE SHE Model and Geographic Information Systems. *Appl. Water Sci.* **2017**, *7*, 591–599. [CrossRef]
67. Papadimitraki, A. The Influence of Spatial Variability of Rainfall to Hydrological Model Fitting—Application to Spercheios River Basin. Diploma Thesis, National Technical University of Athens, Athens, Greece, 2012. (In Greek)
68. Raissis, F.; Theochari, A.; Baltas, E. Hydrological Analysis and Hydraulic Simulation for Sperchios River Basin. In Proceedings of the 17th International Conference on Environmental Science and Technology, CEST 2021, Athens, Greece, 1 September 2021; p. 4.
69. Bournas, A.; Feloni, E.; Bertsioy, M.; Baltas, E. Hydrological and Hydraulic Modelling for a Severe Flood Event in Sperchios River Basin. In Proceedings of the 16th International Conference on Environmental Science and Technology, CEST 2019, Rhodes, Greece, 4 September 2019; p. 2.
70. Zotou, I.; Bellos, V.; Tsihrintzis, V. Calibration Framework for Complex 2D Hydrodynamic Models: Use of Satellite-Derived Flood Extent and Water Depth Data, and Evaluation with Various Performance Metrics. *Adv. Water Resour.* **2025**, *204*, 105066. [CrossRef]
71. Daggupati, P.; Pai, N.; Ale, S.; Douglas-Mankin, K.R.; Zeckoski, R.W.; Jeong, J.; Parajuli, P.B.; Saraswat, D.; Youssef, M.A. A Recommended Calibration and Validation Strategy for Hydrologic and Water Quality Models. *Trans. ASABE* **2015**, *58*, 1705–1719. [CrossRef]
72. Klemes, V. Operational Testing of Hydrological Simulation Models. *Hydrol. Sci. J.* **1986**, *31*, 13–24. [CrossRef]
73. Ndiritu, J. A Comparison of Automatic and Manual Calibration Using the Pitman Model. *Phys. Chem. Earth* **2009**, *34*, 729–740. [CrossRef]
74. Pearson, K., VII. Mathematical Contributions to the Theory of Evolution.—III. Regression, Heredity, and Panmixia. *Philos. Trans. R. Soc. A Math. Phys. Eng. Sci.* **1896**, *187*, 253–318. [CrossRef]
75. Wright, S. Correlation and Causation. *J. Agric. Res.* **1921**, *20*, 557–585.
76. Nash, J.E.; Sutcliffe, J.V. River Flow Forecasting through Conceptual Models. Part I—A Discussion of Principles. *J. Hydrol.* **1970**, *10*, 282–290. [CrossRef]
77. Gupta, H.V.; Kling, H.; Yilmaz, K.K.; Martinez, G.F. Decomposition of the Mean Squared Error and NSE Performance Criteria: Implications for Improving Hydrological Modelling. *J. Hydrol.* **2009**, *377*, 80–91. [CrossRef]
78. Kling, H.; Fuchs, M.; Paulin, M. Runoff Conditions in the Upper Danube Basin under an Ensemble of Climate Change Scenarios. *J. Hydrol.* **2012**, *424–425*, 264–277. [CrossRef]
79. Willmott, C.J. On the Validation of Models. *Phys. Geogr.* **1981**, *2*, 184–194. [CrossRef]
80. Willmott, C.J.; Robeson, S.M.; Matsuura, K. A Refined Index of Model Performance. *Int. J. Climatol.* **2012**, *32*, 2088–2094. [CrossRef]
81. Spyrou, C.; Loupis, M.; Charizopoulos, N.; Apostolidou, I.; Mentzafou, A.; Varlas, G.; Papadopoulos, A.; Dimitriou, E.; Panga, D.; Gkeka, L.; et al. Evaluating Nature-Based Solution for Flood Reduction in Spercheios River Basin under Current and Future Climate Conditions. *Sustainability* **2021**, *13*, 3885. [CrossRef]
82. Dimitriou, E.; Panagiotopoulos, I.; Mentzafou, A.; Anagnostou, C. Assessing the Anthropogenic Impacts on the Fluvial Water and Sediment Fluxes into the Thermaikos Gulf, Northern Greece. *Environ. Eng. Manag. J.* **2018**, *17*, 1053–1068. [CrossRef]
83. Bauer-Gottwein, P.; Christoffersen, L.; Musaeus, A.; Frías, M.; Nielsen, K. Hydraulics of Time-Variable Water Surface Slope in Rivers Observed by Satellite Altimetry. *Remote Sens.* **2024**, *16*, 4010. [CrossRef]
84. Tealdi, S.; Camporeale, C.; Ridolfi, L. Long-Term Morphological River Response to Hydrological Changes. *Adv. Water Resour.* **2011**, *34*, 1643–1655. [CrossRef]
85. Wen, Y.; Li, P.; Li, M.; Ma, C.; Gao, P.; Mu, X.; Zhao, G. Changes in River Cross-Section Morphology and Response to Streamflow and Sediment Processes in Middle Reaches of Yellow River, China. *Chin. Geogr. Sci.* **2025**, *35*, 161–174. [CrossRef]
86. Pörtner, H.; Roberts, D.; Poloczanska, E.; Mintenbeck, K.; Tignor, M.; Alegría, A.; Craig, M.; Langsdorf, S.; Löschke, S.; Möller, V.; et al. Summary for Policymakers. In *Climate Change 2022—Impacts, Adaptation and Vulnerability. Contribution of Working Group II to the Sixth Assessment Report of the Intergovernmental Panel on Climate Change*; Pörtner, H., Roberts, D., Tignor, M., Poloczanska, E., Mintenbeck, K., Alegría, A., Craig, M., Langsdorf, S., Löschke, S., Möller, M., et al., Eds.; Cambridge University Press: Cambridge, UK; New York, NY, USA, 2022; pp. 3–34.
87. O'Neill, B.C.; Kriegler, E.; Ebi, K.L.; Kemp-Benedict, E.; Riahi, K.; Rothman, D.S.; van Ruijven, B.J.; van Vuuren, D.P.; Birkmann, J.; Kok, K.; et al. The Roads Ahead: Narratives for Shared Socioeconomic Pathways Describing World Futures in the 21st Century. *Glob. Environ. Change* **2017**, *42*, 169–180. [CrossRef]
88. Arias, P.A.; Bellouin, N.; Coppola, E.; Jones, R.G.; Krinner, G.; Marotzke, J.; Naik, V.; Palmer, M.D.; Plattner, G.; Rogelj, J.; et al. Technical Summary. In *Climate Change 2021: The Physical Science Basis. Contribution of Working Group I to the Sixth Assessment Report of the Intergovernmental Panel on Climate Change*; Masson-Delmotte, V., Zhai, P., Pirani, A., Connors, S.L., Péan, C., Berger, S., Caud, N., Chen, Y., Goldfarb, L., Gomis, M.I., et al., Eds.; Cambridge University Press: Cambridge, UK; New York, NY, USA, 2023; pp. 35–144.
89. Fricko, O.; Havlik, P.; Rogelj, J.; Klimont, Z.; Gusti, M.; Johnson, N.; Kolp, P.; Strubegger, M.; Valin, H.; Amann, M.; et al. The Marker Quantification of the Shared Socioeconomic Pathway 2: A Middle-of-the-Road Scenario for the 21st Century. *Glob. Environ. Change* **2017**, *42*, 251–267. [CrossRef]

90. Kriegler, E.; Bauer, N.; Popp, A.; Humpenöder, F.; Leimbach, M.; Strefler, J.; Baumstark, L.; Bodirsky, B.; Hilaire, J.; Klein, D.; et al. Fossil-Fueled Development (SSP5): An Energy and Resource Intensive Scenario for the 21st Century. *Glob. Environ. Change* **2017**, *42*, 297–315. [CrossRef]
91. Copernicus Climate Change Service; Climate Data Store CMIP6 Climate Projections. Available online: https://cds.climate.copernicus.eu/ (accessed on 1 February 2025).
92. Zebaze, S.; Anand, A.; Fotso-Nguemo, T.; Taguela, T.; Ngavom, Z.; Komkoua Mbienda, A.; Fotso-Kamga, G.; Choumbou, P.; Vondou, D. Assessing the Performance of the CMIP6 Multi Model Mean in Simulating Precipitation and Temperature across Africa. *Model. Earth Syst. Environ.* **2025**, *11*, 374. [CrossRef]
93. Flato, G.; Marotzke, J.; Abiodun, B.; Braconnot, P.; Chou, S.; Collins, W.; Cox, P.; Driouech, F.; Emori, S.; Eyring, V.; et al. Evaluation of Climate Models. In *Climate Change 2013: The Physical Science Basis. Contribution of Working Group I to the Fifth Assessment Report of the Intergovernmental Panel on Climate Change*; Stocker, T.F., Qin, D., Plattner, G., Tignor, M., Allen, S., Boschung, J., Nauels, A., Xia, Y., Bex, V., Midgley, P., Eds.; Cambridge University Press: Cambridge, UK; New York, NY, USA, 2013; pp. 741–866.
94. Srivastava, A.; Grotjahn, R.; Ullrich, P.A. Evaluation of Historical CMIP6 Model Simulations of Extreme Precipitation over Contiguous US Regions. *Weather Clim. Extrem.* **2020**, *29*, 100268. [CrossRef]
95. Semenov, M.; Stratonovitch, P. Use of Multi-Model Ensembles from Global Climate Models for Assessment of Climate Change Impacts. *Clim. Res.* **2010**, *41*, 1–14. [CrossRef]
96. Eyring, V.; Gillett, N.; Achuta Rao, K.; Barimalala, R.; Barreiro Parrillo, M.; Bellouin, N.; Cassou, C.; Durack, P.; Kosaka, Y.; McGregor, S.; et al. Human Influence on the Climate System. In *Climate Change 2021: The Physical Science Basis. Contribution of Working Group I to the Sixth Assessment Report of the Intergovernmental Panel on Climate Change*; Masson-Delmotte, V., Zhai, P., Pirani, A., Connors, S., Péan, C., Berger, S., Caud, N., Chen, Y., Goldfarb, L., Gomis, M., et al., Eds.; Cambridge University Press: Cambridge, UK; New York, NY, USA, 2021; pp. 423–552.
97. Bi, D.; Dix, M.; Marsland, S.; O'farrell, S.; Sullivan, A.; Bodman, R.; Law, R.; Harman, I.; Srbinovsky, J.; Rashid, H.; et al. Configuration and Spin-up of ACCESS-CM2, the New Generation Australian Community Climate and Earth System Simulator Coupled Model. *J. South. Hemisph. Earth Syst. Sci.* **2020**, *70*, 225–251. [CrossRef]
98. Cherchi, A.; Fogli, P.G.; Lovato, T.; Peano, D.; Iovino, D.; Gualdi, S.; Masina, S.; Scoccimarro, E.; Materia, S.; Bellucci, A.; et al. Global Mean Climate and Main Patterns of Variability in the CMCC-CM2 Coupled Model. *J. Adv. Model. Earth Syst.* **2019**, *11*, 185–209. [CrossRef]
99. Lovato, T.; Peano, D.; Butenschön, M.; Materia, S.; Iovino, D.; Scoccimarro, E.; Fogli, P.G.; Cherchi, A.; Bellucci, A.; Gualdi, S.; et al. CMIP6 Simulations With the CMCC Earth System Model (CMCC-ESM2). *J. Adv. Model. Earth Syst.* **2022**, *14*, e2021MS002814. [CrossRef]
100. Séférian, R.; Nabat, P.; Michou, M.; Saint-Martin, D.; Voldoire, A.; Colin, J.; Decharme, B.; Delire, C.; Berthet, S.; Chevallier, M.; et al. Evaluation of CNRM Earth System Model, CNRM-ESM2-1: Role of Earth System Processes in Present-Day and Future Climate. *J. Adv. Model. Earth Syst.* **2019**, *11*, 4182–4227. [CrossRef]
101. Döscher, R.; Acosta, M.; Alessandri, A.; Anthoni, P.; Arsouze, T.; Bergman, T.; Bernardello, R.; Boussetta, S.; Caron, L.; Carver, G.; et al. The EC-Earth3 Earth System Model for the Coupled Model Intercomparison Project 6. *Geosci. Model Dev.* **2022**, *15*, 2973–3020. [CrossRef]
102. Volodin, E.; Mortikov, E.; Kostrykin, S.; Galin, V.; Lykossov, V.; Gritsun, A.; Diansky, N.; Gusev, A.; Iakovlev, N. Simulation of the Present-Day Climate with the Climate Model INMCM5. *Clim. Dyn.* **2017**, *49*, 3715–3734. [CrossRef]
103. Tatebe, H.; Ogura, T.; Nitta, T.; Komuro, Y.; Ogochi, K.; Takemura, T.; Sudo, K.; Sekiguchi, M.; Abe, M.; Saito, F.; et al. Description and Basic Evaluation of Simulated Mean State, Internal Variability, and Climate Sensitivity in MIROC6. *Geosci. Model Dev.* **2019**, *12*, 2727–2765. [CrossRef]
104. Yukimoto, S.; Kawai, H.; Koshiro, T.; Oshima, N.; Yoshida, K.; Urakawa, S.; Tsujino, H.; Deushi, M.; Tanaka, T.; Hosaka, M.; et al. The Meteorological Research Institute Earth System Model Version 2.0, MRI-ESM2.0: Description and Basic Evaluation of the Physical Component. *J. Meteorol. Soc. Jpn.* **2019**, *97*, 931–965. [CrossRef]
105. Seland, Ø.; Bentsen, M.; Olivié, D.; Toniazzo, T.; Gjermundsen, A.; Graff, L.; Debernard, J.; Gupta, A.; He, Y.; Kirkeväg, A.; et al. Overview of the Norwegian Earth System Model (NorESM2) and Key Climate Response of CMIP6 DECK, Historical, and Scenario Simulations. *Geosci. Model Dev.* **2020**, *13*, 6165–6200. [CrossRef]
106. Kotlarski, S.; Keuler, K.; Christensen, O.B.; Colette, A.; Déqué, M.; Gobiet, A.; Goergen, K.; Jacob, D.; Lüthi, D.; Van Meijgaard, E.; et al. Regional Climate Modeling on European Scales: A Joint Standard Evaluation of the EURO-CORDEX RCM Ensemble. *Geosci. Model Dev.* **2014**, *7*, 1297–1333. [CrossRef]
107. Penman, H.L. Natural Evaporation from Open Water, Bare Soil and Grass. *Proc. R. Soc. A Math. Phys. Eng. Sci.* **1948**, *193*, 120–145. [CrossRef]
108. Hargreaves, G.H.; Samani, Z.A. Reference Crop Evapotranspiration from Temperature. *Appl. Eng. Agric.* **1985**, *1*, 96–99. [CrossRef]
109. Shuttleworth, J. Evaporation. In *Handbook of Hydrology*; Maidment, D.R., Ed.; McGraw-Hill Book Company: New York, NY, USA, 1993; pp. 4.1–4.53.

110. Chen, D.; Rojas, M.; Samset, B.H.; Cobb, K.; Diongue Niang, A.; Edwards, P.; Emori, S.; Faria, S.H.; Hawkins, E.; Hope, P.; et al. Framing, Context, and Methods. In *Climate Change 2021: The Physical Science Basis. Contribution of Working Group I to the Sixth Assessment Report of the Intergovernmental Panel on Climate Change*; Masson-Delmotte, V., Zhai, P., Pirani, A., Connors, S.L., Péan, C., Berger, S., Caud, N., Chen, Y., Goldfarb, L., Gomis, M.I., et al., Eds.; Cambridge University Press: Cambridge, UK; New York, NY, USA, 2021; pp. 147–286.
111. WHO. *WMO Guidelines on the Calculation of Climate Normals*; World Meteorological Organization: Geneva, Switzerland, 2017.
112. WHO; GWP. *Handbook of Drought Indicators and Indices. Integrated Drought Management Programme (IDMP), Integrated Drought Management Tools and Guidelines Series 2*; Svoboda, M., Fuchs, B., Eds.; World Meteorological Organization-Global Water Partnership: Geneva, Switzerland, 2016.
113. Mishra, A.; Singh, V. A Review of Drought Concepts. *J. Hydrol.* **2010**, *391*, 202–216. [CrossRef]
114. Mckee, T.B.; Doesken, N.J.; Kleist, J. The Relationship of Drought Frequency and Duration on Time Scales. In Proceedings of the 8th Conference on Applied Climatology, Anaheim, CA, USA, 17–22 January 1993; pp. 179–183.
115. Vicente-Serrano, S.; Beguería, S.; López-Moreno, J. A Multiscalar Drought Index Sensitive to Global Warming: The Standardized Precipitation Evapotranspiration Index. *J. Clim.* **2010**, *23*, 1696–1718. [CrossRef]
116. WHO. *Standardized Precipitation Index User Guide WMO-No. 1090*; Svoboda, M., Hayes, M., Wood, D., Eds.; World Meteorological Organization: Geneva, Switzerland, 2012.
117. Copernicus European Drought Observatory. *Standardized Precipitation Index (SPI). EDO and GDO Indicator Factsheet*; European Union-Joint Research Centre: Brussels, Belgium, 2025.
118. Copernicus European Drought Observatory. *Standardized Precipitation-Evapotranspiration Index(SPEI) EDO and GDO Indicator Factsheet*; European Union-Joint Research Centre: Brussels, Belgium, 2025.
119. R Core Team. *R: A Language and Environment for Statistical Computing*; R Foundation for Statistical Computing: Vienna, Austria, 2026.
120. Vicente-Serrano, S.; Beguería, S.; López-Moreno, J. *Package "SPEI"*, version 1.8.1; Calculation of the Standardized Precipitation-Evapotranspiration. 2025. Available online: https://spei.csic.es (accessed on 25 August 2026).
121. Beguería, S.; Vicente-Serrano, S.; Reig, F.; Latorre, B. Standardized Precipitation Evapotranspiration Index (SPEI) Revisited: Parameter Fitting, Evapotranspiration Models, Tools, Datasets and Drought Monitoring. *Int. J. Climatol.* **2014**, *34*, 3001–3023. [CrossRef]
122. Hisdal, H.; Tallaksen, L.; Gauster, T.; Bloomfield, J.; Parry, S.; Prudhomme, C.; Wanders, N. Hydrological Drought Characteristics. In *Hydrological Drought: Processes and Estimation Methods for Streamflow and Groundwater*; Tallaksen, L., van Lanen, H., Eds.; Elsevier: Amsterdam, The Netherlands, 2023; pp. 157–231.
123. European Commission. Commission Decision (EU) 2024/721 of 27 February 2024 Establishing, Pursuant to Directive 2000/60/EC of the European Parliament and of the Council, the Values of the Member State Monitoring System Classifications as a Result of the Intercalibration Exercise and Repealing Commission Decision (EU) 2018/229 (Notified under Document C(2024) 1113). *Off. J. Eur. Union* **2024**, *L*, 1–90.
124. European Commission-Joint Research Centre. *Assessment of the Effectiveness of Reported Water Framework Directive Programmes of Measures. Part III, JRC Pressure Indicators v.2.0: Nutrients, Urban Runoff, Flow Regime and Hydromorphological Alteration. EUR 29045 EN*; Pistocchi, A., Aloe, A., Grizzetti, B., Udias, A., Vigiak, O., Bisselink, B., Bouraoui, F., de Roo, A., Gelati, E., Pastori, M., et al., Eds.; Publications Office of The European Union: Luxembourg, 2018.
125. Mentzafou, A.; Katsafados, P.; Papadopoulos, A.; Dimitriou, E. Hydrological Regime Alteration Assessment in the Context of WFD 2000/60: A European and Global Review. *Sustainability* **2023**, *15*, 15704. [CrossRef]
126. Anderson, R. Distribution of the Serial Correlation Coefficient. *Ann. Math. Stat.* **1942**, *13*, 1–13. [CrossRef]
127. Kendall, M.G. *Rank Correlation Methods*; Charles Griffin and Company: London, UK, 1975.
128. Mann, H.B. Nonparametric Tests against Trend. *Econometrica* **1945**, *13*, 245–259. [CrossRef]
129. WHO. *Guide to Hydrological Practices. Volume II Management of Water Resources and Application of Hydrological Practices WMO-No. 168*, 6th ed.; World Meteorological Organization: Geneva, Switzerland, 2009.
130. Hamed, K.; Rao, R. A Modified Mann-Kendall Trend Test for Autocorrelated Data. *J. Hydrol.* **1998**, *204*, 182–196. [CrossRef]
131. Sen, P.K. Estimates of the Regression Coefficient Based on Kendall's Tau. *J. Am. Stat.* **1968**, *63*, 1379–1389. [CrossRef]
132. Benjaminit, Y.; Hochberg, Y. Controlling the False Discovery Rate: A Practical and Powerful Approach to Multiple Testing. *J. R. Stat. Soc. Ser. B (Methodol.)* **1995**, *57*, 289–300. [CrossRef]
133. Pohlert, T. *Trend*, version 1.1.6. Trend: Non-Parametric Trend Tests and Change-Point Detection. 2023. [CrossRef]
134. McLeod, A. *Package "Kendall"*, version 2.2.2. Kendall Rank Correlation and Mann-Kendall Trend Test. 2026. [CrossRef]
135. Ministry of Environment and Energy. *2nd Update of the River Basin Management Plans of River Basin District of Eastern Central Greece (EL07). Analysis of the Anthropogenic Pressures and Their Effect on the Surface and Groundwater Waterbodies*; Ministry of Environment and Energy: Athens, Greece, 2024. (In Greek)

136. Tsaliki, E.; Loison, R.; Kalivas, A.; Panoras, I.; Grigoriadis, I.; Traore, A.; Gourlot, J. Cotton Cultivation in Greece under Sustainable Utilization of Inputs. *Sustainability* **2024**, *16*, 347. [CrossRef]
137. European Commission. *Report from the Commission to the Council and the European Parliament on the Implementation of the Water Framework Directive (2000/60/EC) and the Floods Directive (2007/60/EC) Third River Basin Management Plans Second Flood Risk Management Plans. COM(2025) 2 Final*; European Commission, Directorate-General for Environment: Brussels, Belgium, 2025.
138. European Environment Agency. *European Climate Risk Assessment*; Publications Office of the European Union: Luxembourg, 2024.
139. WBGU. *Opportunities in EU Water Policy: Making the Most of the EU Water Resilience Strategy Policy Paper 14*; WBGU—German Advisory Council on Global Change: Berlin, Germany, 2025.
140. European Commission. *WFD Reporting Guidance 2022 v6.6*; European Commission: Brussels, Belgium, 2023.
141. Wada, Y.; Van Beek, L.; Wanders, N.; Bierkens, M. Human Water Consumption Intensifies Hydrological Drought Worldwide. *Environ. Res. Lett.* **2013**, *8*, 034036. [CrossRef]
142. Ministry of Environment and Energy. *2nd Update of the River Basin Management Plans of River Basin District of Eastern Central Greece (EL07). Program of Basic and Supplementary Measures Including Their Cost-Benefit Analysis*; Ministry of Environment and Energy: Athens, Greece, 2024. (In Greek)
143. Matanó, A.; Hamed, R.; Brunner, M.; Barendrecht, M.; Van Loon, A.; Matanó, A.; Hamed, R.; Brunner, M.; Barendrecht, M. Drought Decreases Annual Streamflow Response to Precipitation, Especially in Arid Regions. *Hydrol. Earth Syst. Sci.* **2025**, *29*, 2749–2764. [CrossRef]
144. Richter, B.; Davis, M.M.; Apse, C.; Konrad, C. A Presumptive Standard for Environmental Flow Protection. *River Res. Appl.* **2012**, *28*, 1312–1321. [CrossRef]
145. Hellenic Republic Standard Environmental Commitments for Projects and Activities in Category B of the 2nd Group Hydraulic Works of Annex II of the Ministerial Decision 1958/2012 (FEK B'21), as Applicable. *Gov. Gaz. Greece* **2013**, *B*, 44115–44142. (In Greek)
146. Reichstein, M.; Benson, V.; Blunk, J.; Camps-Valls, G.; Creutzig, F.; Fearnley, C.; Han, B.; Kornhuber, K.; Rahaman, N.; Schölkopf, B.; et al. Early Warning of Complex Climate Risk with Integrated Artificial Intelligence. *Nat. Commun.* **2025**, *16*, 2564. [CrossRef]
147. Cho, H.; Ackom, E. Artificial Intelligence (AI)-Driven Approach to Climate Action and Sustainable Development. *Nat. Commun.* **2025**, *16*, 1228. [CrossRef]
148. Mahmoud, N.; Kamar, M.; Perez Arredondo, A.; Mtweve, P.; Biber-Freudenberger, L. Nature-Based Solutions for Climate and Health: Mapping Synergies and Trade-Offs. *One Ecosyst.* **2026**, *11*, e164014. [CrossRef]
149. Rasheed, N.; Al-Khafaji, M.; Alwan, I.; Al-Suwaiyan, M.; Doost, Z.; Yaseen, Z. Survey on the Resolution and Accuracy of Input Data Validity for SWAT-Based Hydrological Models. *Heliyon* **2024**, *10*, e38348. [CrossRef]
150. Crawford, N.; Linsley, R. *Digital Simulation in Hydrology: The Stanford Watershed Simulation Model IV: Technical Report No. 39*, Stanford University: Stanford, CA, USA, 1966.
151. Yan, J.; Smith, K. Simulation of Integrated Surface Water and Ground Water Systems—Model Formulation. *Water Resour. Bull.* **1994**, *30*, 879–890. [CrossRef]
152. Zoch, R. On the Relation between Rainfall and Stream Flow. *Mon. Weather Rev.* **1934**, *62*, 315–322. [CrossRef]
153. DHI. *MIKE SHE User Guide and Reference Manual*; DHI: Hørsholm, Denmark, 2023.
154. Ministry of Environment and Energy. *2nd Update of the River Basin Management Plans of River Basin District of Eastern Central Greece (EL07). Management Tools Update Data Collection and Time Series Completion*; Ministry of Environment and Energy: Athens, Greece, 2022. (In Greek)
155. WHO. *Guide to Hydrological Practices. Volume I: Hydrology—From Measurement to Hydrological Information*, 6th ed.; World Meteorological Organization: Geneva, Switzerland, 2008.
156. Thiessen, A.H. Precipitation Averages for Large Areas. *Mon. Weather Rev.* **1911**, *39*, 1082–1089.
157. European Environment Agency Copernicus Land Monitoring Service. CORINE Land Cover CLC2018 Version 2020_20u1. 2018. Available online: https://land.copernicus.eu/pan-european/corine-land-cover/clc2018 (accessed on 5 May 2020).
158. Allen, R.G.; Pereira, L.S.; Raes, D.; Smith, M. *FAO Irrigation and Drainage Paper No. 56. Crop Evapotranspiration (Guidelines for Computing Crop Water Requirements)*; FAO—Food and Agriculture Organization of the United Nations: Rome, Italy, 1998.
159. Hellenic Statistical Authority. *Census of Agricultural and Livestock Holdings 1999–2000*; Hellenic Statistical Authority: Athens, Greece, 2016.
160. Savva, A.P.; Frenken, K. *Crop Water Requirements and Irrigation Scheduling. Irrigation Manual Module 4*; Water Resources Development and Management Office, FAO Sub- Regional office for East and Southern Africa: Harare, Zimbabwe, 2002; Volume 4.
161. Ministry of Environment and Energy National Inventory of Water Abstraction Points of Greece. Available online: http://lmt.ypeka.gr/ (accessed on 1 November 2023).

162. Hellenic Cadastre, S.A. *LSO25 Digital Elevation Model for the LSO25 Ortho Mapping Production. 2m Pixel Size Grid Compilation (1:2,500 Cadastral Tile Distribution)*; Hellenic Cadastre-Directorate of Geospatial Information/Department of Geoinformation: Athens, Greece, 2020.
163. Hellenic Centre for Marine Research. *Development of an Integrated Management System for Basin, Coastal and Marine Zones. Hydrological and Hydrochemical Model of the Under Study Area*; Hellenic Centre for Marine Research-Institute of Marine Biological Resources and Inland Waters; Anavyssos: Attica, Greece, 2015. (In Greek)
164. Ministry of Environment and Energy of Greece. *1st Update of the Flood Risk Management Plan of the River Basin District of Eastern Central Greece (EL07) Analysis of Area Characteristics and Flood Mechanisms*; Ministry of Environment and Energy of Greece: Athens, Greece, 2023. (In Greek)
165. Rawls, W.J.; Ahuja, L.R.; Brakensiek, D.L.; Shirmohammadi, A. Infiltration and Soil Water Movement. In *Handbook of Hydrology*; Maidment, D., Ed.; McGraw-Hill: New York, NY, USA, 1993; pp. 5.1–5.51.
166. Hignett, C.; Evett, S. Direct and Surrogate Measures of Soil Water Content. In *Field Estimation of Soil Water Content. A Practical Guide to Methods, Instrumentation and Sensor Technology. Training Course Series No. 30*; International Atomic Energy Agency: Vienna, Austria, 2008; pp. 1–22.
167. Batu, V. *Aquifer Hydraulics: A Comprehensive Guide to Hydrogeologic Data Analysis*; John Wiley & Sons, Inc.: New York, NY, USA, 1998.
168. Enemark, T.; Pareta, K.; Jensen, K. Evaluating Conceptual Configurations of the Linear Reservoir Module of the MIKE SHE Modelling System. *SSRN* **2023**, 1–37. [CrossRef]
169. Moriasi, D.; Arnold, J.; Van Liew, M.; Bingner, R.; Harmel, R.; Veith, T. Model Evaluation Guidelines for Systematic Quantification of Accuracy in Watershed Simulations. *Trans. ASABE* **2007**, *50*, 885–900. [CrossRef]
170. Krause, P.; Boyle, D.P.; Bäse, F. Comparison of Different Efficiency Criteria for Hydrological Model Assessment. *Adv. Geosci.* **2005**, *5*, 89–97. [CrossRef]
171. Onyutha, C. Pros and Cons of Various Efficiency Criteria for Hydrological Model Performance Evaluation. In *Proceedings of the International Association of Hydrological Sciences*; Copernicus Publications: Göttingen, Germany, 2024; Volume 385, pp. 181–187.
172. Legates, D.; Mccabe, G. Evaluating the Use of "Goodness-of-Fit" Measures in Hydrologic and Hydroclimatic Model Validation. *Water Resour. Res.* **1999**, *35*, 233–241. [CrossRef]
173. Chai, T.; Draxler, R.R. Root Mean Square Error (RMSE) or Mean Absolute Error (MAE)?—Arguments against Avoiding RMSE in the Literature. *Geosci. Model Dev.* **2014**, *7*, 1247–1250. [CrossRef]
174. Gupta, H.; Sorooshian, S.; Yapo, P.O. Status of Automatic Calibration for Hydrologic Models: Comparison with Multilevel Expert Calibration. *J. Hydrol. Eng.* **1999**, *4*, 135–143. [CrossRef]
175. Knoben, W.; Freer, J.; Woods, R. Technical Note: Inherent Benchmark or Not? Comparing Nash-Sutcliffe and Kling-Gupta Efficiency Scores. *Hydrol. Earth Syst. Sci.* **2019**, *23*, 4323–4331. [CrossRef]
176. McCuen, R.; Knight, Z.; Cutter, G. Evaluation of the Nash-Sutcliffe Efficiency Index. *J. Hydrol. Eng.* **2006**, *11*, 597–602. [CrossRef]
177. Moriasi, D.; Gitau, M.; Pai, N.; Daggupati, P. Hydrologic and Water Quality Models: Performance Measures and Evaluation Criteria. *Trans. ASABE* **2015**, *58*, 1763–1785. [CrossRef]
178. Bland, J.; Altman, D. Statistical Methods for Assesing Agreement between Two Methods of Clinical Measurement. *Lancet* **1986**, *327*, 307–310. [CrossRef]
179. Giavarina, D. Understanding Bland Altman Analysis. *Biochem. Med.* **2015**, *25*, 141–151. [CrossRef]
180. Bisselink, B.; Bernhard, J.; Gelati, E.; Adamovic, M.; Guenther, S.; Mentaschi, L. *Impact of a Changing Climate, Land Use, and Water Usage on Europe's Water Resources: A Model Simulation Study*; EUR 29130 EN. JRC110927; Publications Office of the European Union: Luxembourg, 2018.
181. Sarigil, G.; Cavus, Y.; Aksoy, H.; Eris, E. Frequency Curves of High and Low Flows in Intermittent River Basins for Hydrological Analysis and Hydraulic Design. *Stoch. Environ. Res. Risk Assess.* **2024**, *38*, 3079–3092. [CrossRef]
182. Smakhtin, V. Low Flow Hydrology: A Review. *J. Hydrol.* **2001**, *240*, 147–186. [CrossRef]
183. Meylan, P.; Favre, A.-C.; Musy, A. *Predictive Hydrology. A Frequency Analysis Approach*; CRC Press, Taylor & Francis Group: New York, NY, USA, 2011.
184. Helsel, D.; Hirsch, R.; Ryberg, K.; Archfield, S.; Gilroy, E. *Statistical Methods in Water Resources: U.S. Geological Survey Techniques and Methods, Book 4, Chap. A3*; U.S. Department of the Interior, U.S. Geological Survey: Reston, VA, USA, 2020.
185. Singh, A.; Singh, A.; Engelhardt, M. *Some Practical Aspects of Sample Size and Power Computations for Estimating the Mean of Positively Skewed Distributions in Environmental Applications*; EPA/600/s-99/006; United States Environmental Protection Agency: Washington, DC, USA, 1999.
186. Hinkle, D.; Wiersma, W.; Jurs, S. *Applied Statistics for the Behavioral Sciences*, 5th ed.; Houghton Mifflin: Boston, MA, USA, 2003.
187. Hellenic Cadastre LSO25 (25cm) Orthophotos. Available online: https://gis.ktimanet.gr/gis/map/ (accessed 5 on May 2026).
188. Cadastre Hellenic. *LSO Project (Large Scale Orthophotos) (50cm) Orthophotos*; Hellenic Cadastre: Holargos, Greece, 2020.

189. Kakavas, N. Hydrological Balance of the Sperkhios River Basin (Central Greece). Ph.D. Thesis, University of Athens & Institute of Geological and Mining Research, Athens, Greece, 1984. (In Greek)
190. Ministry of Development. *Development of Management Plans and Tools for Eastern Greece Water District. Phase A, Deliverable 07-A-III-1. Geology—Hydrogeology*; Ministry of Development: Athens, Greece, 2006. (In Greek)

Disclaimer/Publisher's Note: The statements, opinions and data contained in all publications are solely those of the individual author(s) and contributor(s) and not of MDPI and/or the editor(s). MDPI and/or the editor(s) disclaim responsibility for any injury to people or property resulting from any ideas, methods, instructions or products referred to in the content.